Steepestdescent moment method for threedimensional magnetohydrodynamic equilibria

S. P. Hirshman and J. C. Whitson

Related Articles

Implementation of an in-vessel calibration light source for JET
Rev. Sci. Instrum. 83, 10D505 (2012)

A new neutral particle analyzer diagnostic and its first commissioning on HL-2A
Rev. Sci. Instrum. 83, 10D702 (2012)

Tangential x-ray imaging crystal spectrometer on J-TEXT tokamak
Rev. Sci. Instrum. 83, 10E502 (2012)

C-III flow measurements with a coherence imaging spectrometer
Rev. Sci. Instrum. 83, 10E102 (2012)

Thick-wall effects in the theory of resistive wall modes
Phys. Plasmas 19, 062503 (2012)

Additional information on Phys. Fluids

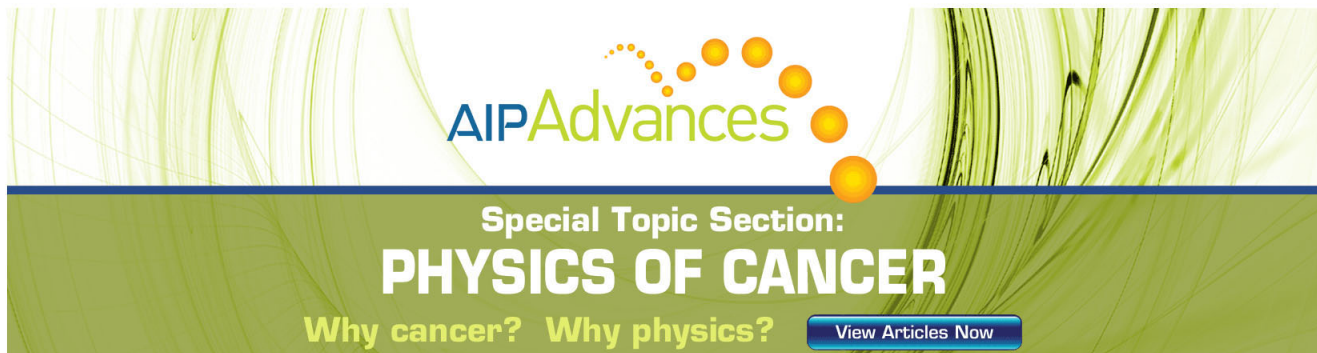Journal Homepage: http://pof.aip.org/

Journal Information: http://pof.aip.org/about/about_the_journal

Top downloads: http://pof.aip.org/features/most_downloaded

Information for Authors: http://pof.aip.org/authors

Steepest-descent moment method for three-dimensional magnetohydrodynamic equilibria

S. P. Hirshman

Oak Ridge National Laboratory, Oak Ridge, Tennessee 37830

J. C. Whitson

UCC-ND Computer Sciences, Oak Ridge, Tennessee 37830

An energy principle is used to obtain the solution of the magnetohydrodynamic (MHD) equilibrium equation $\mathbf{J} \times \mathbf{B} - \nabla p = 0$ for nested magnetic flux surfaces that are expressed in the inverse coordinate representation $\mathbf{x} = \mathbf{x}(\rho, \theta, \zeta)$. Here, θ and ζ are poloidal and toroidal flux coordinate angles, respectively, and $p = p(\rho)$ labels a magnetic surface. Ordinary differential equations in ρ are obtained for the Fourier amplitudes (moments) in the doubly periodic spectral decomposition of $\mathbf{x}$. A steepest-descent iteration is developed for efficiently solving these nonlinear, coupled moment equations. The existence of a positive-definite energy functional guarantees the monotonic convergence of this iteration toward an equilibrium solution (in the absence of magnetic island formation). A renormalization parameter λ is introduced to ensure the rapid convergence of the Fourier series for $\mathbf{x}$, while simultaneously satisfying the MHD requirement that magnetic field lines are straight in flux coordinates. A descent iteration is also developed for determining the self-consistent value for λ.

I. INTRODUCTION

The global analysis of finite-aspect-ratio, high-beta, three-dimensional (3-D) toroidal configurations with complex external coil configurations of the type envisioned for fusion reactor applications generally requires numerical methods. The variational formulation of magnetohydrodynamic (MHD) equilibria[1,2] provides a mathematically efficient prescription for treating the truncation or closure of an approximate finite-series solution of the nonlinear equilibrium equations. Also inherent in any energy principle is an iteration scheme for obtaining the solution of this truncated set of equations, which is based on seeking the minimum energy state.

The practical application of variational principles for obtaining numerical equilibria has progressed recently, so that there are currently fully 3-D codes based on either Eulerian[3] or Lagrangian[4] formulations. Both of these methods are numerically inefficient in comparison with moment methods that have been previously applied to two-dimensional (2-D) problems arising in systems with an ignorable spatial coordinate[5] or that result from averaging 3-D equilibria.[6] This has prompted the present formulation of 3-D moment equilibria, as well as an alternate approach[7] based on the variational principle of Grad.[2]

The moment expansion of the plasma equilibrium results in a finite set of coupled, nonlinear, ordinary differential equations for the Fourier amplitudes of the inverse mapping[8] $\mathbf{x} = \mathbf{x}(\rho, \theta, \zeta)$, where (ρ, θ, ζ) are flux coordinates, ρ labels the flux surfaces (constant pressure contours), and θ and ζ are poloidal and toroidal angle variables, respectively. In the present paper, a steepest-descent procedure is developed for solving the nonlinear moment equations that arise in MHD equilibrium problems. This is the Fourier space formulation of the numerical scheme used in Ref. 4.

The success of moment methods is attributable in part to the rapid convergence of the Fourier series for the inverse equilibrium coordinates. In the present formulation, this convergence property is ensured by introducing a renormalization parameter (Sec. II) to distinguish between the geometric and the magnetic poloidal angles (the latter describes straight magnetic field lines).

The MHD energy principle[1] is used in Sec. III to obtain the equilibrium equations in a conservative form. It is shown that the variational moment equations correspond to the spectral coefficients of the covariant components of the MHD force. In Sec. IV, the Fourier decomposition of the inverse mapping is introduced, and the steepest-descent method of solution for the moment amplitudes is derived. The boundary conditions at the magnetic axis and at the plasma edge are discussed in Sec. V, and the descent algorithm is generalized to include a vacuum region surrounding the plasma. The moment representation of an analytic 2-D equilibrium is given in Sec. VI to clarify the role of the poloidal angle θ. Some details of the numerical techniques used to solve the inverse equations are given in Sec. VII. A Galerkin method for treating the magnetic axis and plasma shift is described in Sec. VIII, and some numerical results are presented in Sec. IX.

The equilibria calculated here have a single magnetic axis. By applying magnetic perturbations of the form $\mathbf{B} = \nabla \times A_{\parallel} \mathbf{B}_0$, where $A_{\parallel} = \Sigma_{m,n} A_{mn}(\rho) \exp[i(m\theta - n\zeta)]$, it is possible to investigate the stability of these equilibria to a more general class of (tearing) perturbations.

II. EQUILIBRIUM EQUATIONS IN FLUX COORDINATES

The equations describing MHD equilibrium of a static (no fluid flow), isotropic plasma are the force balance equation and Ampere's and Gauss's laws:

$$\mathbf{F} \equiv -\,\mathbf{J} \times \mathbf{B} + \nabla p = 0, \tag{1a}$$

$$\nabla \times \mathbf{B} = \mu_0 \mathbf{J}, \tag{1b}$$

$$\nabla \cdot \mathbf{B} = 0, \tag{1c}$$

where $p = p(\rho)$ is the pressure and ρ is a radial coordinate labeling a magnetic flux surface. The quantity $\mathbf{F}$ is the residual MHD force, which must vanish in equilibrium. For the nested toroidal flux surface geometry considered here, flux coordinate angles θ and ζ may be introduced, where θ is a poloidal angle ($\Delta\theta = 2\pi$ once the short way around the magnetic axis) and ζ is a toroidal angle ($\Delta\zeta = 2\pi$ once the long way around the torus). The conditions $\mathbf{B} \cdot \nabla p = 0$ and $\nabla \cdot \mathbf{B} = 0$ can be satisfied by writing $\mathbf{B}$ in contravariant form as follows[1]:

$$\mathbf{B} = \nabla\zeta \times \nabla\chi + \nabla\Phi \times \nabla\theta^*$$
$$= B^\theta \mathbf{e}_\theta + B^\zeta \mathbf{e}_\zeta, \tag{2}$$

where $2\pi\chi(\rho)$ and $2\pi\Phi(\rho)$ are, respectively, the poloidal and toroidal magnetic fluxes enclosed between the magnetic surface labeled ρ and the magnetic axis ($\rho = 0$, where $\nabla\chi = 0$),

$$\theta^* = \theta + \lambda(\rho, \theta, \zeta) \tag{3a}$$

is the poloidal angle that makes the magnetic field lines straight[9] [i.e., the local rotation number $\mathbf{B} \cdot \nabla\theta^*/\mathbf{B} \cdot \nabla\zeta$ is a function of ρ alone in the (ρ, θ^*, ζ) coordinate system], and λ is a periodic function of θ and ζ with zero average over a magnetic surface, $\iint d\theta\, d\zeta\, \lambda = 0$. The contravariant basis vectors are $\mathbf{e}^i \equiv \nabla\alpha_i$, where $\alpha = (\rho, \theta, \zeta)$, and the covariant basis vectors are $\mathbf{e}_i \equiv \partial\mathbf{x}/\partial\alpha_i = \sqrt{g}\,\mathbf{e}^j \times \mathbf{e}^k$, where (i, j, k) forms a positive triplet, and $\sqrt{g} = (\nabla\rho \cdot \nabla\theta \times \nabla\zeta)^{-1}$ is the Jacobian. Thus, from Eq. (2), the contravariant components of the magnetic field are $B^i \equiv \mathbf{B} \cdot \mathbf{e}^i$, where

$$B^\theta = \frac{1}{\sqrt{g}}\left(\chi' - \Phi'\frac{\partial\lambda}{\partial\zeta}\right), \tag{3b}$$

$$B^\zeta = \frac{1}{\sqrt{g}}\,\Phi'\left(1 + \frac{\partial\lambda}{\partial\theta}\right), \tag{3c}$$

$B^\rho = 0$, and the prime denotes $\partial/\partial\rho$. The covariant components $B_i \equiv \mathbf{B} \cdot \mathbf{e}_i$ are related to B^i through the metric tensor $g_{ij} \equiv \mathbf{e}_i \cdot \mathbf{e}_j$:

$$B_i = B^\theta g_{\theta i} + B^\zeta g_{\zeta i}, \tag{3d}$$

as can be verified by taking the scalar product of Eq. (2) with $\mathbf{e}_i$.

Although the function $\lambda(\rho, \theta, \zeta)$ in Eq. (3a) can be eliminated[9] by taking $\theta = \theta^*$, its retention here provides flexibility in specifying the poloidal angle θ. The role of the poloidal angle in the moment expansion of equilibria is to yield rapidly convergent[5] Fourier series for the spatial coordinates $\mathbf{x}(\rho, \theta, \zeta)$. Since only truncated series are used in practice, a proper choice for θ is necessary to provide adequate accuracy in the approximate moment solution. In general, this value for θ is incompatible with the requirement that magnetic field lines are straight in (θ^*, ζ) coordinates. The inclusion of λ therefore generates a convergent resummation of the inverse equilibrium Fourier moment expansion. In this context, λ assumes the role of a renormalization parameter.

Inserting Eq. (2) into Eq. (1a) yields

$$\mathbf{F} = F_\rho \nabla\rho + F_\beta\, \beta, \tag{4a}$$

where

$$F_\rho = \sqrt{g}(J^\zeta B^\theta - J^\theta B^\zeta) + p', \tag{4b}$$

$$F_\beta = J^\rho, \tag{4c}$$

$\beta = \sqrt{g}\,(B^\zeta \nabla\theta - B^\theta \nabla\zeta)$ and $J^i \equiv \mathbf{J} \cdot \nabla\alpha_i = \mu_0^{-1}\nabla \cdot (\mathbf{B} \times \nabla\alpha_i)$. There are only two independent components of $\mathbf{F}$, since the component $\mathbf{B} \cdot \mathbf{F} = p'\mathbf{B} \cdot \nabla\rho = 0$ is already incorporated into the representation of $\mathbf{B}$ in Eq. (2). Writing J^i in terms of the covariant components of $\mathbf{B}$ yields expressions for the forces in terms of the flux functions, χ', Φ', and p', and the metric:

$$F_\rho = \mu_0^{-1}\left(B^\theta\frac{\partial B_\theta}{\partial\rho} + B^\zeta\frac{\partial B_\zeta}{\partial\rho} - \mathbf{B} \cdot \nabla B_\rho\right) + p', \tag{4d}$$

$$F_\beta = \frac{1}{\mu_0\sqrt{g}}\left(\frac{\partial B_\zeta}{\partial\theta} - \frac{\partial B_\theta}{\partial\zeta}\right). \tag{4e}$$

Here, for any scalar A, the derivative along a magnetic field line is

$$\mathbf{B} \cdot \nabla A \equiv B^\theta\frac{\partial A}{\partial\theta} + B^\zeta\frac{\partial A}{\partial\zeta}. \tag{4f}$$

In the 2-D axisymmetric case,[5,8] $F_\beta = 0$ can be integrated to yield

$$B_\zeta = F(\rho). \tag{5a}$$

Noting that $g_{\theta\zeta} = g_{\rho\zeta} = 0$ and $\partial\lambda/\partial\zeta = 0$, due to axisymmetry, and $B^\zeta = B_\zeta/g_{\zeta\zeta}$ with $g_{\zeta\zeta} = R^2$ (where R is the major radius, see Fig. 1), Eq. (4d) becomes the inverse Grad-
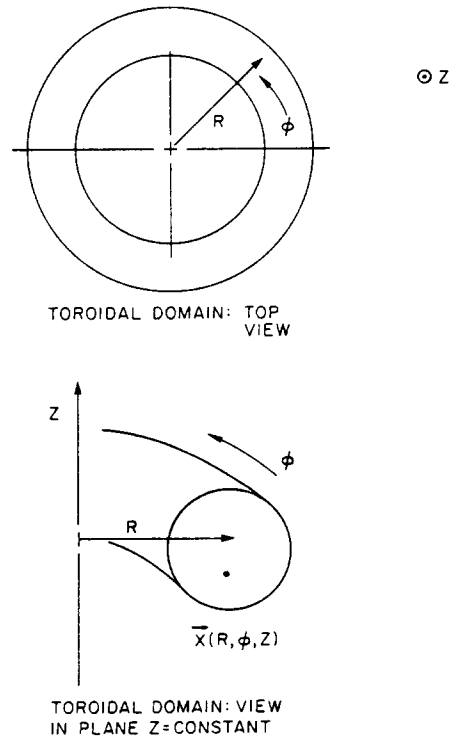

TOROIDAL DOMAIN: TOP VIEW

TOROIDAL DOMAIN: VIEW IN PLANE Z = CONSTANT

FIG. 1. Toroidal-cylindrical coordinate system.

Shafranov equation:

$$F_\rho = \frac{\chi'}{\mu_0\sqrt{g}}\left[\frac{\partial}{\partial\rho}\left(\frac{\chi' g_{\theta\theta}}{\sqrt{g}}\right) - \frac{\partial}{\partial\theta}\left(\frac{\chi' g_{\rho\theta}}{\sqrt{g}}\right)\right] + \frac{FF'}{\mu_0 R^2} + p'.$$

(5b)

From Eqs. (3c) and (3d), note that Eq. (5a) can be written $(\Phi'R^2/\sqrt{g})(1 + \partial\lambda/\partial\theta) = F(\rho)$, which yields $\Phi'(\rho) = \langle\sqrt{g}/R^2\rangle F(\rho)$ and

$$\frac{\partial\lambda}{\partial\theta} = \frac{\sqrt{g}/R^2}{\langle\sqrt{g}/R^2\rangle} - 1.$$

(5c)

Here, brackets denote a normalized θ average.

Equation (5c) shows that in 2-D geometry, the straight magnetic field line system for $\lambda = 0$ is one for which $\sqrt{g}/R^2$ is constant on a magnetic surface. Consider an equilibrium that is approximated by shifted, elliptical flux surfaces for which the cylindrical coordinates (R, Z) have the low-order Fourier representation $R = R_0(\rho) + R_1(\rho)\cos\theta$, $Z = Z_1(\rho)\sin\theta$. Analysis[8] of this configuration indicates that to leading order in the inverse aspect ratio, the condition $\partial(R^2/\sqrt{g})/\partial\theta = 0$ in the (ρ, θ) coordinate system leads to an unphysical inward shift $\Delta = R_0(0) - R_0(\rho) < 0$ which is independent of the plasma pressure. The retention of λ allows for the surface variation of $\sqrt{g}/R^2$ in the (ρ, θ) coordinate system, where the low-order Fourier series representation for (R, Z) is appropriate. It also yields the correct variation[5] of $R_0(\rho)$ with pressure. An explicit analytic calculation of λ illustrating this behavior is given in Sec. VI.

III. ENERGY PRINCIPLE IN THE INVERSE COORDINATE REPRESENTATION

A variational principle[1] for obtaining the equilibrium equation (1) is based on the plasma energy

$$W = \int\left(\frac{|B|^2}{2\mu_0} + \frac{p}{\gamma - 1}\right)d^3x,$$

(6)

where $\gamma \geq 0$ is the adiabatic index. Equation (6) can be shown to be stationary with respect to virtual displacements of B and p that preserve the magnetic flux and mass density profiles.[1,3] For $\gamma = 0$, W reduces to the Lagrangian (a nondefinite form) introduced by Grad.[2]

The scalar invariance[5] of W can be used to compute it directly in flux coordinates. It is then natural to introduce the inverse representation, for which the real space coordinates x are considered to be the *dependent* variables and the flux coordinates $\alpha \equiv (\rho, \theta, \zeta)$ are treated as independent variables during the variation of W. In this representation, the flux and mass conservation constraints must be incorporated into the expressions for B and p. Equation (2) already conserves the magnetic flux profiles $\chi'(\rho)$ and $\Phi'(\rho)$. The adiabatic conservation of mass between neighboring flux surfaces requires[1]

$$p(\rho) = M(\rho)(V')^{-\gamma},$$

(7)

where $V'(\rho) = \int\int d\theta\,d\zeta\,|\sqrt{g}|$ is the differential volume element. Here, the mass function $M(\rho)$ is fixed during the variation of $p(\rho)$ in Eq. (6), whereas $V'(\rho)$, which depends on the

geometry of the flux surfaces, may vary. Thus, the energy evaluated in flux coordinates is

$$W = \int\frac{|B|^2}{2\mu_0}|\sqrt{g}|d^3\alpha + \int_0^1\frac{M(\rho)}{\gamma - 1}(V')^{1-\gamma}d\rho,$$

(8a)

where

$$|B|^2 \equiv B^iB_i = (B^\theta)^2g_{\theta\theta} + 2B^\theta B^\zeta g_{\theta\zeta} + (B^\zeta)^2g_{\zeta\zeta},$$

(8b)

$d^3\alpha = d\rho\,d\theta\,d\zeta$, and the outermost flux surface is $\rho = 1$. Summation over repeated Roman indices is implied.

For the toroidal configurations under consideration, a cylindrical coordinate system $x = (R, \phi, Z)$ is appropriate, where R is the major radius, ϕ is the toroidal angle, and Z is the height above the midplane (Fig. 1). It then follows that the metric tensor elements are

$$g_{ij} = R_iR_j + R^2\phi_i\phi_j + Z_iZ_j,$$

(9a)

where $R_i = \partial R/\partial\alpha_i$, etc., and $(\alpha_1, \alpha_2, \alpha_3) = (\rho, \theta, \zeta)$. The Jacobian is

$$\sqrt{g} = R\det(G_{ij}),$$

(9b)

$$G_{ij} = \frac{\partial x_i}{\partial\alpha_j},$$

(9c)

where $(x_1, x_2, x_3) = (R, \phi, Z)$. Henceforth, it is assumed that $\sqrt{g} > 0$ (i.e., there is only a single magnetic axis). Inserting the metric elements into Eq. (8b) yields a cylindrical representation for $|B|^2$,

$$|B|^2 = \frac{b_R^2 + R^2b_\phi^2 + b_Z^2}{(\sqrt{g})^2},$$

(10)

where $b_i \equiv \sqrt{g}B\cdot\nabla x_i = b^\theta(\partial x_i/\partial\theta) + b^\zeta(\partial x_i/\partial\zeta)$ are the cylindrical polar components of B and $(b^\theta, b^\zeta) = \sqrt{g}(B^\theta, B^\zeta)$.

To perform the variation of W, suppose that in addition to being functions of the flux coordinates, the cylindrical coordinates x and the renormalization parameter λ also depend on an artificial time parameter t. Then, for any scalar function $S(x, \lambda)$, $\dot{S} \equiv \partial S/\partial t = (\partial S/\partial x_i)\dot{x}_i + (\partial S/\partial\lambda)\dot{\lambda}$. Then, the "time derivative" (i.e., variation) of W in Eq. (8) becomes

$$\frac{dW}{dt} = \int\left[-\left(\frac{|B|^2}{2\mu_0} + p\right)\frac{\partial\sqrt{g}}{\partial t} + \frac{1}{\mu_0\sqrt{g}}(b_R\,\dot{b}_R + R^2b_\phi\,\dot{b}_\phi + b_Z\,\dot{b}_Z + Rb_\phi^2\,\dot{R})\right]d^3\alpha.$$

(11)

Here, $M(\rho)$, $\chi'(\rho)$, and $\Phi'(\rho)$ were held fixed in deriving Eq. (11).

The variation of the polar components of B is

$$\dot{b}_j = b^\theta\frac{\partial\dot{x}_j}{\partial\theta} + b^\zeta\frac{\partial\dot{x}_j}{\partial\zeta} + \dot{b}^\theta\frac{\partial x_j}{\partial\theta} + \dot{b}^\zeta\frac{\partial x_j}{\partial\zeta},$$

(12a)

where $\dot{b}^\alpha(\lambda) = b^\alpha(\dot{\lambda})$. Next, the variation of the Jacobian can be obtained by differentiating Eq. (9b):

$$\frac{\partial\sqrt{g}}{\partial t} = \frac{\dot{R}}{R}\sqrt{g} + \sqrt{g}\left(\frac{\partial\dot{x}_i}{\partial\alpha_j}\frac{\partial\alpha_j}{\partial x_i}\right),$$

(12b)

where $(\sqrt{g}/R)\partial\alpha_i/\partial x_j$ is the classical adjoint of G_{ij} (transpose of the cofactors), which is $(\sqrt{g}/R)$ times the inverse of G_{ij}:

$$\frac{\sqrt{g}}{R}\frac{\partial \alpha_i}{\partial x_j} = \begin{pmatrix} \phi_\theta \, Z_\zeta - \phi_\zeta \, Z_\theta & R_\zeta \, Z_\theta - R_\theta \, Z_\zeta & R_\theta \, \phi_\zeta - R_\zeta \, \phi_\theta \\ \phi_\zeta \, Z_\rho - \phi_\rho \, Z_\zeta & R_\rho \, Z_\zeta - R_\zeta \, Z_\rho & R_\zeta \, \phi_\rho - R_\rho \, \phi_\zeta \\ \phi_\rho \, Z_\theta - \phi_\theta \, Z_\rho & R_\theta \, Z_\rho - R_\rho \, Z_\theta & R_\rho \, \phi_\theta - R_\theta \, \phi_\rho \end{pmatrix}. \tag{12c}$$

Using Eq. (12) in Eq. (11) yields

$$\frac{dW}{dt} = -\int F_i \dot{x}_i \, d^3\alpha - \int F_\lambda \dot{\lambda} \, d^3\alpha$$
$$- \int_{\rho=1} |\sqrt{g}| \frac{\partial p}{\partial x_i}\left(\frac{|B|^2}{2\mu_0} + p\right)\dot{x}_i \, d\theta \, d\zeta. \tag{13}$$

Here, the MHD force components F_i are

$$F_i = -\frac{\partial}{\partial \alpha_i}\left[|\sqrt{g}|\frac{\partial \alpha_j}{\partial x_i}\left(\frac{|B|^2}{2\mu_0} + p\right)\right]$$
$$+ \mu_0^{-1}|\sqrt{g}|\nabla \cdot [(\Lambda_i \mathbf{B} \cdot \nabla x_i)\mathbf{B}]$$
$$+ \delta_{i1}\frac{|\sqrt{g}|}{R}\left(\frac{|B|^2}{2\mu_0} + p - \frac{R^2(\mathbf{B} \cdot \nabla\phi)^2}{\mu_0}\right), \tag{14a}$$

where $\Lambda_1 = \Lambda_3 = 1$, $\Lambda_2 = R^2$ [the index "i" is fixed and not summed in Eq. (14a)], and

$$F_\lambda = \Phi'|\sqrt{g}|F_\beta. \tag{14b}$$

The last term in Eq. (13) is the energy change due to the moving plasma boundary. In Eq. (14), each of the quantities $|B|^2$, $\sqrt{g}$, and $\partial \alpha_j/\partial x_i$ is to be expressed in inverse coordinates as given by Eqs. (8)–(10) and (12c), and $(F_1, F_2, F_3) = (F_R, F_\phi, F_Z)$. Also, $\mathbf{x}$ is to be considered a function of $\boldsymbol{\alpha}$. For example, $\mathbf{B} \cdot \nabla x_i$ is given explicitly after Eq. (10).

The identity $\nabla \cdot (\mathbf{e}_i^{\text{cyl}}/R) = 0$, which can also be written

$$\frac{\partial}{\partial \alpha_j}\left(\frac{\sqrt{g}}{R}\frac{\partial \alpha_j}{\partial x_i}\right) = 0, \tag{15}$$

may be used to express F_i in terms of the forces F_ρ and F_β previously defined in Eq. (4) (here $\mathbf{e}_i^{\text{cyl}} \equiv \partial \mathbf{x}/\partial x_i$):

$$F_i = -|\sqrt{g}|\left[\frac{\partial p}{\partial x_i}F_\rho + \left(b^\zeta \frac{\partial \theta}{\partial x_i} - b^\theta \frac{\partial \zeta}{\partial x_i}\right)F_\beta\right]. \tag{16}$$

It follows from Eqs. (4a) and (16) that $-F_i/|\sqrt{g}|$ is the covariant component (in the cylindrical coordinate basis) of the MHD residual force.

For the toroidal systems under consideration here, $\Phi' \neq 0$ (except at $\rho = 0$). It is then possible to choose[4] $\phi = \zeta$. This choice for the magnetic toroidal angle, which is adopted here, simplifies the algebraic structure of Eq. (14), effectively yielding a 2-D Jacobian,

$$\sqrt{g} = RG, \tag{17a}$$

$$G = R_\theta Z_\rho - R_\rho Z_\theta, \tag{17b}$$

and thus reduces the complexity of solving Eq. (14) numerically. In particular, no ζ derivatives appear in $\sqrt{g}$ once ζ is fixed. In addition, the equation $F_\phi = 0$ is redundant, since it follows from Eq. (16) that for $\sqrt{g} \neq 0$, F_ρ and F_β are linear combinations of F_R and F_Z when $\phi = \zeta$. Thus, for a fixed boundary plasma, W is stationary when the MHD equilibri-

um equations $F_\rho = F_\beta = 0$ are satisfied. This proves the energy principle in inverse coordinates for the toroidal angle choice $\phi = \zeta$.

Two-dimensional inverse equilibrium equations $F_i = 0$ were originally derived from a variational principle in Ref. 5 in a form similar to Eq. (16) with $F_\beta = 0$ and were subsequently generalized to three dimensions in Ref. 7. There are, however, several advantages associated with retaining the conservative form of F_i given in Eq. (14). Since F_i is a second-order differential operator in flux coordinates, a conservative finite-difference representation for F_i (in ρ) is readily derived by integrating Eq. (14) on a radial mesh. Spectral analysis of F_i is facilitated by integrating Eq. (14) by parts in θ and ζ (see Sec. VII). In this way, no derivatives of R, Z, or λ higher than first order are required for the numerical evaluation of F_i. Finally, the boundary condition at a free boundary $(\rho = 1)$, which requires the continuity of the total pressure, is easily implemented when F_i is in a conservative form.

In contrast to the axisymmetric case, where $F_\lambda = 0$ may be analytically integrated [cf. Eq. (5a)], in three dimensions it is necessary to solve this equation numerically. From Eq. (4e), it is apparent that the relation $F_\lambda = 0$ is a *linear* elliptic equation for λ on each flux surface. As noted previously, by introducing λ in Eq. (2), the number of Fourier harmonics required for an accurate inverse representation of $\mathbf{x}(\rho, \theta, \zeta)$ is reduced. Since the Fourier coefficients of $\mathbf{x}$ satisfy moments of the *nonlinear* equations $F_i = 0$ (see Sec. IV), the introduction of λ actually simplifies the solution of the equilibrium problem by accelerating the convergence of the Fourier series for $\mathbf{x}$, even though additional linear equations must be solved.

With the *magnetic* toroidal angle ζ chosen equal to the *geometric* toroidal angle ϕ, the conservative expressions for the two force components F_R and F_Z become particularly simple:

$$F_R = \frac{\partial}{\partial \rho}(Z_\theta P) - \frac{\partial}{\partial \theta}(Z_\rho P)$$
$$+ \mu_0^{-1}\left(\frac{\partial}{\partial \theta}(B^\theta b_R) + \frac{\partial}{\partial \zeta}(B^\zeta b_R)\right)$$
$$+ G\left(\frac{P}{R} - \frac{(RB^\zeta)^2}{\mu_0}\right), \tag{18a}$$

$$F_Z = -\frac{\partial}{\partial \rho}(R_\theta P) + \frac{\partial}{\partial \theta}(R_\rho P)$$
$$+ \mu_0^{-1}\left(\frac{\partial}{\partial \theta}(B^\theta b_Z) + \frac{\partial}{\partial \zeta}(B^\zeta b_Z)\right), \tag{18b}$$

where $P = R(p + |B|^2/2\mu_0)$ and b_i is defined after Eq. (10).

Note from Eqs. (14b) and (16) that when the angle renormalization parameter λ is retained, the equations for R, Z, and λ are dependent, since there are only two independent MHD forces F_ρ and F_β. This underdetermination is resolved

by specifying the poloidal angle variable θ. The choice of θ adopted here, which is dictated by the economization of the finite Fourier expansions for R and Z and is different from previous angle specifications,[4,5,7] is described in the Appendix.

IV. STEEPEST-DESCENT METHOD OF SOLUTION FOR THE MOMENT EQUATIONS

The inverse mapping $\mathbf{x} = \mathbf{x}(\rho, \theta, \zeta)$ can be expressed as an explicit function of the flux coordinates as follows:

$$R = R_0(\rho) + p_R(\rho, \theta, \zeta), \tag{19a}$$

$$Z = Z_0(\rho) + p_Z(\rho, \theta, \zeta). \tag{19b}$$

Here, p_j (for $j = 1,3$) are periodic functions of the angles, that is, $\iint d\theta\, d\zeta\, p_j = 0$. The moment representation of the equilibrium results from expanding p_j and λ in Fourier series. Defining $(x_1, x_2, x_3) \equiv (R, \lambda, Z)$, where λ now replaces the fixed toroidal angle $\phi = \zeta$ as a coordinate, and introducing the associated complex Fourier amplitudes X_j^{mn}, Eq. (19) becomes

$$x_j = \sum_{m, n} X_j^{mn}(\rho)\exp[i(m\theta - n\zeta)]. \tag{20}$$

The reality of x_j implies $X_j^{mn} = (X_j^{-m, -n})^*$. Since λ is periodic, $X_2^{00} = 0$.

Using the representation of x_j given in Eq. (20), the variation of the energy in Eq. (13) becomes (neglecting the surface terms)

$$\frac{dW}{dt} = - \int (F_j^{mn})^* \frac{\partial X_j^{mn}}{\partial t}\, dV, \tag{21a}$$

where

$$F_j^{mn} = (V')^{-1} \iint F_j \exp[-i(m\theta - n\zeta)]d\theta\, d\zeta, \tag{21b}$$

$F_1 = F_R$, $F_2 = F_\lambda$, $F_3 = F_Z$, and $dV = V'\, d\rho$. The volume factor $V' = \partial V/\partial \rho$ normalizes the force coefficients to ensure the correct asymptotic dependence on ρ at the magnetic axis $(\rho = 0)$ and in practice is chosen to be the differential volume V_i' corresponding to the initial plasma state.

The Fourier coefficients $F_j^{mn} = (F_j^{-m, -n})^*$ are the variational forces that must vanish in equilibrium.[5,7] By considering the moment amplitudes X_j^{mn} as independent trial functions in a Ritz method (subject to the reality constraint), it is seen that the equations $F_j^{mn} = 0$ represent the most accurate system for determining the X_j^{mn} that result from a finite truncation of the series in Eq. (20). Previously, this system of nonlinear, second-order, ordinary differential equations has been solved in two dimensions by direct Jacobian inversion methods.[5,7] In three dimensions, the larger number of moment amplitudes needed to describe an equilibrium can significantly decrease the efficiency and numerical stability of such direct methods. Therefore, an iteration method is now developed for following the path, in the phase space of the moment amplitudes, along which $\dot{W}$ decreases at a maximum rate.

Since W is bounded from below due to flux and mass $(p^{1/\gamma})$ conservation and is positive definite for $\gamma > 1$, the equilibrium corresponds to a minimum energy state.[1] Thus, by finding the path along which $\dot{W}$ decreases monotoni-

cally, an equilibrium will eventually be reached. To minimize $\dot{W}$ in Eq. (21a), note that $\Sigma_j |\int F_j^* \dot{x}_j\, dV|^2 \leqslant \int \Sigma_j |F_j|^2\, dV \int \Sigma_j |\dot{x}_j|^2\, dV$, with equality pertaining if and only if $\dot{x}_j = kF_j$, where k is an arbitrary real constant ($k = 1$ here). Thus, the descent path is

$$\frac{\partial X_j^{mn}}{\partial t} = F_j^{mn}, \tag{22a}$$

and the maximum rate of decrease in W along this path is given by

$$\frac{dW}{dt} = - \sum_{j, m, n} \int |F_j^{mn}|^2\, dV. \tag{22b}$$

Equation (22) comprises the descent equations for relaxing W to its minimum energy state. It is the Fourier space analog of the descent equations derived in Ref. 4. Note that $\dot{W} = 0$ if and only if $F_j^{mn} = 0$ for all j, m, and n (that is, when all the equilibrium equations are satisfied simultaneously).

Since the F_j^{mn} correspond to second-order differential operators in ρ, the descent equation (22a) comprises a set of parabolic differential equations. The convergence to an equilibrium solution is prohibitively slow[10,11] for an explicitly differenced version of Eq. (22a). Implicit schemes,[11] which remove the small time step required for stability of explicit schemes, are impractical here since the forces F_j^{mn} are such nonlinear functions of the amplitudes X_j^{mn}. The convergence of these equations can be accelerated, while retaining an explicit form for the forces, by converting them to hyperbolic equations[10] (the second-order Richardson scheme):

$$\frac{\partial^2 X_j^{mn}}{\partial t^2} + \frac{1}{\tau} \frac{\partial X_j^{mn}}{\partial t} = F_j^{mn}. \tag{23}$$

The parameter $\tau > 0$ has little effect on the stability of the numerical scheme[10] and can therefore be chosen to maximize the decay rate of the least-damped mode of Eq. (23), thereby minimizing the number of iterations required to reach steady state. The optimum value for τ, leading to critical damping in Eq. (23), is[10]

$$\frac{1}{\tau_{0p}} \simeq - \frac{d}{dt}\left(\ln \int |F|^2\, dV\right), \tag{24}$$

where $\int |F|^2\, dV \equiv \int \Sigma_{j, m, n} |F_j^{mn}|^2\, dV$. There is an energy principle associated with the second-order system equation (23). Multiplying Eq. (23) by $V_i'(\dot{X}_j^{mn})^*$, taking complex conjugates, and using Eq. (21a) for $\dot{W}$ yields

$$\frac{d}{dt}(W_K + W) = - \frac{2}{\tau} W_K, \tag{25}$$

where $W_K = \int |\dot{X}|^2/2\, dV$ is the kinetic energy. Thus, for $\tau > 0$, the sum of the kinetic and potential energies, which is bounded from below, decays monotonically until $W_K = 0$ and equilibrium is attained.

V. BOUNDARY AND INITIAL CONDITIONS

The magnetic axis ($\rho = 0$) is a singular curve of the coordinate system where $\nabla \chi = 0$. For toroidally nested surfaces, this corresponds to the one parameter space curve $R = R_0(\zeta)$, $Z = Z_0(\zeta)$. The geometry of the magnetic axis is

S. P. Hirshman and J. C. Whitson

determined by Taylor-expanding χ in $x = R - R_0$ and $y = Z - Z_0$:

$$\chi = \alpha(\zeta)x^2 + 2\beta(\zeta)xy + \gamma(\zeta)y^2 + \ldots, \tag{26}$$

where $\alpha\gamma - \beta^2 > 0$ for elliptical surfaces encircling the magnetic axis. In terms of the moment amplitudes this implies (for $j = 1,3$)

$$X_j^{mn}(\rho = 0, t) = 0, \quad m \neq 0. \tag{27a}$$

In fact, if $V(\rho) = \int_0^\rho V' \, d\rho$ is the volume inside a flux surface, then $X_j^{mn} \sim V^{m/2}$ as $\rho \to 0$. Since the magnetic axis corresponds to an extremum of the flux (or pressure) contours, the radial variation of $[R_0(\zeta), Z_0(\zeta)]$ must be second order near $\rho = 0$. Hence, for $j = 1,3$,

$$\frac{dX_j^{0n}}{d\rho}(\rho = 0, t) \sim \lim_{\rho \to 0} V'(\rho). \tag{27b}$$

For the typical case when $\rho \sim \sqrt{V}$, Eq. (27b) reduces to $(X_j^{0n})' = 0$. For $j = 2(x_2 = \lambda)$, the origin boundary condition may be deduced by noting from Eq. (4e), together with the fact that R_θ and Z_θ both vanish at the magnetic axis, that

$$\lim_{V \to 0} \lambda_\theta = \frac{\sqrt{g}}{\oint \sqrt{g} \, d\theta} - 1. \tag{27c}$$

Equations (27a) and (27b) imply $R = R_0(\zeta) + \rho[r_1(\zeta)\cos\theta + r_2(\zeta)\sin\theta] + O(\rho^2)$, with a similar expansion for Z, and hence $\sqrt{g} = V'[g_0(\zeta) + V^{1/2}g_1(\theta, \zeta)]$. Since $g_0(\zeta)$ is independent of θ, Eq. (27c) yields $\partial X_2^{mn}(\rho = 0, t)/\partial\theta = 0$. The boundary conditions given here are different from those in Ref. 4, due to the polar representation used there.

Now consider two types of boundary conditions that may be imposed at the plasma edge.

A. Fixed boundary

In this case, the shape of the outermost flux surface $(\rho = 1)$ is fixed for all times. When the poloidal angle renormalization parameter λ is retained, this is equivalent to prescribing the individual Fourier harmonics of both R and Z at $\rho = 1$ (see the Appendix):

$$X_j^{mn}(\rho = 1, t) = X_{jb}^{mn}, \tag{28}$$

for $j = 1,3$. No boundary condition is needed for $x_2 = \lambda$, since F_λ is local in ρ (there are no radial derivatives of λ in F_λ). In this representation, the angle coordinate λ accounts for the rotation of the magnetic field lines in the poloidal direction during the minimization of W.

B. Free boundary

The position of the free plasma boundary is determined by the continuity of the total pressure $|B|^2/2\mu_0 + p$ at the plasma–vacuum interface $(\rho = 1)$ and by the vanishing of the normal component of the vacuum field over this surface. These boundary conditions can be incorporated into the variational principle[1,4] by appending the vacuum magnetic energy to the plasma energy W_{pl} given in Eq. (8). The total energy functional then becomes

$$W = W_{pl} - W_v = \int_{plasma}\left(\frac{|B|^2}{2\mu_0} + p\right)d^3x$$
$$- \int_{vacuum}\frac{|\nabla v|^2}{2\mu_0} d^3x, \tag{29}$$

where $\mathbf{B}_v = -\nabla v$ is the vacuum magnetic field. (This representation for $\mathbf{B}_v$ conserves the total plasma and vacuum coil currents.) The minus sign in Eq. (29) guarantees the continuity of the total pressure at the plasma–vacuum interface. In the plasma, where the magnetic flux is conserved on each flux surface, a change in the position of the boundary produces a reciprocal variation in the energy. [Thus, there is a minus sign in the last term of Eq. (13).] In general, the vacuum region will contain current-carrying coils surrounded by a conducting wall. The vacuum integral in Eq. (29) must then be separated into regions bounded by the coil surfaces, with appropriate jumps in v to account for the coil currents.

Taking the time derivative of Eq. (29) and using Eq. (13) to evaluate the plasma energy change yields

$$\frac{dW}{dt} = -\int F_i \dot{x}_i \, d^3\alpha + \mu_0^{-1}\int_{vacuum} \dot{v}F_v \, d^3x$$
$$- \int_{\rho=1} S_i \dot{x}_i \, d\theta \, d\zeta$$
$$- \mu_0^{-1}\left(\int_{\rho=1} \dot{v}\mathbf{B}_v \cdot d\mathbf{S}_\rho - \int_{wall} \dot{v}\mathbf{B}_v \cdot d\mathbf{S}\right), \tag{30}$$

where

$$S_i = \left[|\sqrt{g}|\frac{\partial\rho}{\partial x_i}\left(\frac{|B|^2}{2\mu_0} + p - \frac{|\nabla v|^2}{2\mu_0}\right)\right]_{\rho=1} \tag{31a}$$

is the pressure jump at the plasma–vacuum interface, $|B|^2$ is the magnetic field strength in the plasma given by Eq. (8b), $d\mathbf{S}_\rho = \nabla\rho|\sqrt{g}|d\theta \, d\zeta$, and

$$F_v \equiv -\nabla \cdot \mathbf{B}_v = \nabla^2 v \tag{31b}$$

is the vacuum "force." The last term in S_i represents the vacuum energy change due to the motion of the free boundary. Thus, the descent equation for the vacuum potential is

$$\dot{v} = F_v. \tag{31c}$$

Equation (30) is a minimax principle for the plasma–vacuum equilibrium configuration. The physical boundary conditions, which require $\mathbf{B}_v \cdot d\mathbf{S}_\rho = 0$ and $S_i = 0$ at $\rho = 1$ and $\mathbf{B}_v \cdot d\mathbf{S} = 0$ at the conducting wall, are also natural boundary conditions for the extremization of W.

Now, consider the initial conditions needed to integrate Eq. (23). Both X_j^{mn} and $\dot{X}_j^{mn}$ must be prescribed at the beginning of the descent. To guarantee that W will decrease at $t = 0$, it is convenient to take

$$\dot{X}_j^{mn} = \alpha F_j^{mn}. \tag{32a}$$

In practice, $\alpha \simeq 0$ provides a sufficiently well-behaved start for the descent equations. The initial profiles $X_j^{mn}(\rho)$ are chosen consistent with the boundary conditions at $\rho = 0$ and $\rho = 1$. From Eqs. (27) and (28), it follows that for $j \neq 2$,

$$X_j^{mn}(\rho, 0) = \begin{cases} v(\rho)X_{jb}^{mn}, & m \neq 0, \\ X_{jb}^{0n}, & m = 0, \end{cases} \tag{32b}$$

where X_{jb}^{mn} are the initial boundary data. For $j = 2$, $\lambda^{mn} = X_2^{mn}(\rho, 0) = 0$ is used in practice.

In Eq. (32b), $v(\rho)$ is a monotonic function of ρ satisfying $v(1) = 1$ and $v(0) = 0$. [A small boundary layer near the magnetic axis where $X_j^{mn} \sim V^{m/2}$ is neglected by the ansatz in Eq. (32b).] Geometrically, $v(\rho)$ is simply related to the initial plasma volume in an equivalent infinite-aspect-ratio system $(R \to \infty)$:

$$v(\rho) = [V_\infty (\rho,0)/V_\infty (1,0)]^{1/2}, \tag{32c}$$

where $V_\infty = R_m \int G \, d\theta \, d\zeta$. Here, G is the 2-D Jacobian defined in Eq. (17b), and R_m is the mean radius of the magnetic axis. The radial grid can be adjusted by choosing the functional form for $v(\rho)$. For example, $v(\rho) = \rho$ identifies ρ with the usual polar radius, whereas $v(\rho) = \rho^{1/2}$ makes ρ a measure of the volume inside a flux surface.[4]

There are other possible ways of choosing ρ. For tokamaks and stellarators with strong uniform toroidal magnetic fields, $\Phi(\rho)$ is monotonic and a magnetic prescription

$$\rho = [\Phi(\rho)/\Phi(1)]^{1/2} \tag{32d}$$

can be used. In Refs. 5 and 7, $-\rho$ was chosen to be the $\cos \theta$ harmonic of R. The poloidal flux $\chi'(\rho)$ was then determined from the surface-averaged force balance equation, $\langle \sqrt{g} F_\rho \rangle \equiv \int\int \sqrt{g} F_\rho \, d\theta \, d\zeta = 0$, which results from varying the energy with respect to χ at fixed $\iota(\chi)$ and $p(\chi)$. This equation is not, however, independent of the other moment equations $F_j^{mn} = 0$. Indeed, Eq. (16) can be used to show that

$$\langle \sqrt{g} F_\rho \rangle = - \sum_{m, n} [(X_R^{mn})'(F_R^{mn})^* + (X_Z^{mn})'(F_Z^{mn})^*].$$

Thus, the various prescriptions for ρ are related, but only those given by Eqs. (32c) and (32d) preserve the symmetry of the descent equations.

Once the radial coordinate is specified, the initial magnetic and pressure profiles can be chosen so that the surface-averaged pressure balance equation $\langle \sqrt{g} F_\rho \rangle = 0$ will be satisfied at $t = 0$. (In the 2-D problem considered in Ref. 5, the average pressure balance was satisfied at all times by changing from magnetic flux to current flux variables. This procedure does not, however, generalize to three dimensions.) For example, for fixed ι and p profiles, the toroidal flux Φ may be rescaled with respect to ρ so that the average pressure balance

$$\langle (\sqrt{g} \mathbf{J} \cdot \nabla \zeta)(\sqrt{g} \mathbf{B} \cdot \nabla \theta) \rangle - \langle (\sqrt{g} \mathbf{J} \cdot \nabla \theta)(\sqrt{g} \mathbf{B} \cdot \nabla \zeta) \rangle$$
$$+ \mu_0 p' V' = 0, \tag{33a}$$

where $\langle A \rangle = \int\int d\theta \, d\zeta \, A$ and $V' = \langle \sqrt{g} \rangle$, is initially satisfied. This generally improves the convergence rate of the descent algorithm. Using the explicit forms for B^θ and B^ζ given in Eq. (3), integrating the λ_θ and λ_ζ derivative terms by parts, and assuming $F_\beta \simeq 0$, Eq. (33a) becomes

$$\chi' J_\zeta' - \Phi' J_\theta' + \mu_0 p' V' = 0, \tag{33b}$$

where $J_\theta' \equiv \langle \sqrt{g} \mathbf{J} \cdot \nabla \theta \rangle = - \partial \langle B_\zeta \rangle / \partial \rho$ and $J_\zeta' \equiv \langle \sqrt{g} \mathbf{J} \cdot \nabla \zeta \rangle = \partial \langle B_\theta \rangle / \partial \rho$ are the current fluxes. Equation (33b) is exact when $F_\beta = 0$ or $\lambda = 0$. Assuming that the pressure and rotational transform profiles are prescribed functions of the initial volume $v(\rho)$, so that $\chi' = \iota(v)\Phi'$ and $p' = (\partial p/\partial v)(\partial v/\partial \rho)$, Eq. (33b) becomes a linear first-order differential equation for $h(\rho)$, where $\Phi'(\rho) = (\partial v/\partial \rho)$

$\times [2h(\rho)]^{1/2}$ and h is regular at $\rho = 0$,

$$\frac{\partial}{\partial \rho}[(\iota^2 \hat{g}_{\theta\theta} + 2\iota \hat{g}_{\theta\zeta} + \hat{g}_{\zeta\zeta})h] + (\iota^2 \hat{g}_{\theta\theta}' + 2\iota \hat{g}_{\theta\zeta}' + \hat{g}_{\zeta\zeta}')h$$
$$+ \mu_0 p_v V' = 0. \tag{34}$$

Here, $\hat{g}_{ij} \equiv (\partial v/\partial \rho)\langle g_{ij}/\sqrt{g} \rangle$, $p_v = \partial p/\partial v$, and $\sqrt{g} = R(\partial v^2/\partial \rho)G(\theta, \zeta)$.

Equation (33b) provides a practical numerical criterion for the convergence to an equilibrium. Forming the quantity

$$Q \equiv \frac{\chi' J_\zeta' - \Phi' J_\theta' + \mu_0 p' V'}{|\chi' J_\zeta'| + |\Phi' J_\theta'| + \mu_0 |p'| V'}, \tag{35}$$

note that a converged equilibrium is attained when Q is less than the spatial discretization error.

VI. MOMENT ANALYSIS OF SOLOV'EV EQUILIBRIUM

An exact analytic solution of a 2-D equilibrium problem[12] in the inverse coordinate representation will now be considered. This will emphasize the importance of distinguishing between the geometric angle θ appearing in the Fourier representation of the flux surfaces and the magnetic angle $\theta^* = \theta + \lambda$ [Eq. (3a)], which describes straight magnetic field lines. A solution of the axisymmetric Grad–Shafranov equation,[12] when the magnetic field is represented as $\mathbf{B} = \chi' \nabla \zeta \times \nabla \rho + F(\rho)\nabla \zeta$, is

$$\rho^2 = \frac{\beta_1}{\chi_0^2}\left[Z^2 R_0^2 + \left(\frac{\beta_0}{8\beta_1}\right)(R^2 - R_m^2)^2 \right], \tag{36}$$

where $\chi' = 2\rho\chi_0$ (ρ^2 is the normalized poloidal flux, $0 < \rho < 1$), $p(\rho) = \beta_0(1 - \rho^2)$, and $F^2 = R_0^2(1 - 4\beta_1\rho^2)$. The toroidal field is normalized to unity if R_0 is identified with the mean major radius. Note that $R = R_m$ is the magnetic axis, which is determined by the boundary curve $\rho = 1$. The spectral analysis of Eq. (36) is trivial in terms of the variables $u = R^2$ and Z, yielding

$$u = R_m^2 - \chi_0(8/\beta_0)^{1/2}\rho \cos \theta, \tag{37a}$$

$$Z = (\chi_0/R_0)\beta_1^{-1/2}\rho \sin \theta. \tag{37b}$$

Here, θ is a geometric angle yielding a rapidly convergent Fourier expansion for R and Z, which is not equal to the magnetic angle θ^* in which field lines are straight. To show this, note that the Jacobian is

$$\sqrt{g} = (\chi_0^2/R_0)(2/\beta_0\beta_1)^{1/2}\rho. \tag{38}$$

Thus, $\sqrt{g}/R^2$ is not a function of ρ alone, as Eq. (5c) requires for $\lambda = 0$. Therefore, even though the geometric solution given in Eq. (37) satisfies the equilibrium Grad–Shafranov equation, it apparently fails to simultaneously satisfy $J^\rho = F_\beta = 0$ when $\lambda = 0$. By introducing the angle renormalization parameter λ, the angle θ can be chosen for its geometric properties while the constraint $F_\beta = 0$ is satisfied by λ. For the present example, it is easy to evaluate λ explicitly from Eq. (5c):

$$\lambda_\theta = (1 - a^2)^{1/2}/(1 - a \cos \theta) - 1, \tag{39a}$$

where $a(\rho) = \chi_0(8/\beta_0)^{1/2}\rho/R_m^2 < 1$. Thus, $\lambda = \Sigma_{m=1} \lambda_m \times \sin m\theta$, where

$$\lambda_m = (2/m)\{[1 - (1 - a^2)^{1/2}]/a\}^m. \tag{39b}$$

Note that for $a^2 < 1$, λ_m decays exponentially with m. Similarly, the magnetic flux profile is found to be

$$\frac{\Phi'}{\chi'} \equiv q(\rho) = \frac{\chi_0}{R_m^2} \left[\frac{1}{2\beta_0 \beta_1} \left(\frac{1 - 4\beta_1 \rho^2}{1 - a^2} \right) \right]^{1/2}. \qquad (40)$$

The results in Eqs. (38)–(40) provide an analytic basis for testing the computational methods developed here (see Sec. IX). They also reveal the fundamental incompatibility, in the absence of angle renormalization, between an economical Fourier description of the flux surface geometry and the MHD constraint, $J^\rho = 0$.

VII. NUMERICAL METHOD

In this section, some numerical aspects of solving the descent equations are considered. First, the time discretization of Eq. (23) is discussed, and an estimate for the maximum stable time step is obtained. Then, the spatial discretization of the forces F_j^{mn} is performed, including the incorporation of the boundary conditions considered in Sec. V.

A. Time discretization

The descent equation (23) for the plasma can be written

$$\frac{d}{dt} S(t) \dot{X}_j^{mn} = S(t) F_j^{mn}, \qquad (41)$$

where $S(t) = \exp \int^t \tau^{-1} dt'$. Integrating Eq. (41) from $t = t_{n-1/2}$ to $t = t_{n+1/2}$, where t_n is the time at the nth iteration, yields

$$\dot{X}_j^{mn}(t_{n+1/2}) = (1 - b_n) \dot{X}_j^{mn}(t_{n-1/2})$$
$$+ (1 - \tfrac{1}{2} b_n) \Delta t F_j^{mn}(t_n), \qquad (42a)$$

where $\Delta t = t_{n+1/2} - t_{n-1/2}$,

$$\dot{X}_j^{mn}(t_{n+1/2}) = \frac{X_j^{mn}(t_{n+1}) - X_j^{mn}(t_n)}{\Delta t} + O(\Delta t^2) \qquad (42b)$$

is the discretized "velocity," and

$$b_n = 1 - \exp\left(-\int_{t_{n-1/2}}^{t_{n+1/2}} \frac{1}{\tau} dt \right) \qquad (42c)$$

is the incremental damping factor. Using the expression for $1/\tau$ given in Eq. (24) and adding a small minimum damping rate $(\tau^{-1})_{\min}$ (to guarantee convergence near the energy minimum[3]) yields

$$b_n = 1 - y_n(1 - b_{\min}), \qquad (42d)$$

where $y_n = \min(\langle F^2 \rangle_n / \langle F^2 \rangle_{n-1}, \langle F^2 \rangle_{n-1} / \langle F^2 \rangle_n)$, $b_{\min} = (\tau^{-1})_{\min} \Delta t$, and $\langle F^2 \rangle_n = \int |F(t_n)|^2 dV$. With this form for b_n, Eq. (42a) reduces to the conjugate gradient part of the Fletcher–Reeves algorithm used in Ref. 3. In practice, since b_n is proportional to the algebraically largest eigenvalue of $\mathbf{F}$, y_n should be averaged[4] over several iterations to reduce the effect of a mixture of eigenvectors. Since the longest damping time scales as $N_\rho \Delta t$, where N_ρ is the number of radial mesh points, an average over N_ρ previous iterations is approximately equivalent to averaging over one e-folding decay time.

The maximum stable time step Δt may be estimated from a von Neumann analysis[11] of the linearized version of

Eq. (42a). The result is

$$\Delta t_{\max} = (4/\lambda_{\max})^{1/2}, \qquad (43)$$

where $|\lambda_{\max}|$ is the modulus of the algebraically smallest eigenvalue of $\mathbf{F}$. Equation (43) is $(|\lambda_{\max}|)^{1/2} > 1$ times larger than the stable time step for an equivalent first-order time scheme.

To estimate $\lambda_{\max}$, consider the eigenvalues of the spatially discretized and linearized operator $\mathbf{F}$. Noting that the shortest radial wavelengths in the F_R and F_Z operators will determine $\lambda_{\max}$, the eigenvalue condition can be approximated by using only the highest-order ρ derivatives in Eq. (18). Denoting the k th eigenvector by (R_k, Z_k), Eq. (18) reduces in the short-wavelength limit to

$$D_{RR} R_k'' - D_{RZ} Z_k'' = -\lambda_k R_k, \qquad (44a)$$

$$-D_{RZ} R_k'' + D_{ZZ} Z_k'' = -\lambda_k Z_k, \qquad (44b)$$

where $D_{RR} = Z_\theta^2 d_0$, $D_{RZ} = Z_\theta R_\theta d_0$, $D_{ZZ} = R_\theta^2 d_0$, $d_0 = R |B|^2/(GV_i' \mu_0)$, and $G = \sqrt{g}/R$. For short-wavelength modes, the diffusion coefficients in Eq. (44) can be treated as constants (in a WKB sense). The spatial discretization for the second-order derivatives in Eq. (44) is taken to be

$$R''(\rho = \rho_n) \simeq [R(\rho_{n+1}) - 2R(\rho_n) + R(\rho_{n-1})]/(\Delta\rho)^2, \qquad (45)$$

and similarly for Z'', where $\Delta\rho = \rho_n - \rho_{n-1}$ is the uniform radial grid spacing. Letting $R_k(n) = R_0 \exp(in\beta_0)$, where β_0 is a real phase factor, it is apparent that $R_k''(n) = -4R_k(n)\sin^2(\beta_0/2)/(\Delta\rho)^2$. Using this result and applying Gerschgorin's theorem[11] to account for a nonuniform ρ dependence of the diffusion coefficients, it follows from Eq. (44) that

$$\max_k |\lambda_k| \leqslant [4/(\Delta\rho)^2] \max_{\rho, \theta, \zeta} \left\{ [\max(D_{RR}, D_{ZZ})]^{1/2} \right.$$

$$\left. \times (D_{RR}^{1/2} + D_{ZZ}^{1/2}) \right\} \simeq \frac{4\hat{g}_{\theta\theta}}{(\Delta\rho)^2} \left(\frac{|B|^2}{2\mu_0} \right), \qquad (46)$$

where $\hat{g}_{\theta\theta} = 2Rg_{\theta\theta}/(GV_i')$. Obviously, λ_k^{-1} is related to the time for an Alfvén wave to travel across the radial mesh. Note that $\Delta\rho = (N_\rho - 1)^{-1}$, which implies $\max|\lambda_k| \sim N_\rho^2$. When the cylindrical nature of the eigenfunctions of Eq. (44) is accounted for, it is found that $\Delta\rho$ in Eq. (46) is replaced by $(N_\rho + M/2 - 1)^{-1}$, where M is the maximum poloidal mode number.

It is now possible to make a heuristic comparison between the steepest-descent method and the Jacobian inversion methods used previously[5,7] to solve the equilibrium moment equations. The Jacobian methods involve inverting the linearized $\mathbf{F}$ operator and hence determining all the eigenvalues of this operator. In contrast, the steepest-descent method requires only a bound for the largest eigenvalue of $\mathbf{F}$. When the number of eigenvalues is large (i.e., for a stiff system), an accurate inversion of $\mathbf{F}$ becomes prohibitively time-consuming, and the accelerated-descent method seems preferable.

B. Spatial discretization of the forces

The continuous expressions for the MHD residual forces obtained in Secs. III and IV may be transformed into

discrete forms by numerical integration of W.[13] Discrete conservative forms for the Fourier-transformed forces are then obtained by varying the individual nodal amplitudes.[4] The asymptotic behavior of the solutions near the magnetic axis is used to appropriately modify these nodal equations in the vicinity of $\rho = 0$.

The angle integrals in Eq. (8) are replaced by discrete sums as follows[13]:

$$W \equiv \int d\rho \iint w(\rho, \theta, \zeta) d\theta \, d\zeta$$

$$\rightarrow \int d\rho \sum_{i=1}^{N_T} \sum_{j=1}^{N_Z} w(\rho, \theta_{i-1/2}, \zeta_{j-1/2}) \Delta\theta \, \Delta\zeta, \quad (47a)$$

where $\Delta\theta = 2\pi/N_T$, $\Delta\zeta = 2\pi/N_Z$ (N_T and N_Z are the number of discrete θ and ζ mesh points, respectively), $\theta_{i-1/2} = (i - 1/2)\Delta\theta$, $\zeta_{j-1/2} = (j - 1/2)\Delta\zeta$, and

$$w = RG [|B|^2/2\mu_0 + p/(\gamma - 1)] \quad (47b)$$

is the energy density functional evaluated at the angular half-mesh points, where $\sqrt{g} = RG$, $p = M(\rho)(V')^{-\gamma}$, and

$$V'(\rho) = \sum_i \sum_j \sqrt{g}(\rho, \theta_{i-1/2}, \zeta_{j-1/2}) \Delta\theta \, \Delta\zeta. \quad (47c)$$

A rectangle integration rule accurate to second order in $\Delta\theta$ and $\Delta\zeta$ was used in Eq. (47a). Because this rule preserves the discrete orthogonality of the trigonometric functions, it is more accurate[14] in the present problem than certain nominally higher-order schemes (e.g., Simpson's rule or Gaussian quadrature). If there are M theta modes and N zeta modes in the spectrum of R, Z, and λ, then $N_T = 2M + 1$ and $N_Z = 2N + 1$ are the minimum number of points required in the sum in Eq. (47a). (This estimate assumes that the modes are consecutive and counts $M \geqslant 0$, $N \geqslant 0$.)

The Fourier analysis of the coordinates R, Z, and λ appearing in the energy density w permits an *exact* evaluation of w at the half-mesh points $(\theta_{i-1/2}, \zeta_{j-1/2})$. It is this interpolation property of the trigonometric functions, together with the application of fast transform techniques, that makes harmonic analysis desirable even for the very nonlinear equilibrium problem under consideration here.[15]

What remains in Eq. (47a) is now a one-dimensional integration in ρ. Consider the set of N_ρ discrete radial mesh points (nodes) $\rho_k \equiv (k - 1)\Delta\rho$ for $k = 1, ..., N_\rho$, where $\Delta\rho = (N_\rho - 1)^{-1}$. The Fourier coefficients $X_\alpha^{mn}(\rho = \rho_k)$ for $\alpha = (R, \lambda, Z)$ will be denoted $X_\alpha^{mn}(k)$. They are the *nodal amplitudes*, which are to be obtained as the solution to the discrete force equations. In analogy with the angle discretization in Eq. (47), it is useful to introduce the radial half-mesh points $\rho_{k+1/2} = (\rho_k + \rho_{k+1})/2$, for $k = 1, ..., N_\rho - 1$. Then, the ρ integration in Eq. (47a) becomes

$$W = \sum_{k=1}^{N_\rho - 1} \sum_{i=1}^{N_T} \sum_{j=1}^{N_Z} w(\rho_{k+1/2}, \theta_{i-1/2}, \zeta_{j-1/2}) \Delta\rho \, \Delta\theta \, \Delta\zeta.$$

$$(48)$$

Henceforth, for brevity, the angular subscripting is suppressed. To evaluate w at the radial half-mesh points, central sum and difference formulas[13] can be used: $X_\alpha(k + 1/2) = [X_\alpha(k) + X_\alpha(k + 1)]/2$ and $X'_\alpha(k + 1/2) = [X_\alpha(k + 1) - X_\alpha(k)]/\Delta\rho$. Since w depends only on X_α

and X'_α, but no higher-order radial derivatives, these relations are sufficient to discretize w.

The discrete forces are obtained by taking the time derivatives of the nodal amplitudes $X_\alpha^{mn}(k, t)$ appearing in the discrete form for W, in exact analogy with the procedure developed in Sec. III for the continuous case. The result is not unique, since several radial discretizations of w, all of which agree to $O(\Delta\rho^2)$, are possible. The particular discrete form for w used here was chosen to minimize the radial coupling between the nodal amplitudes, which is desirable both for numerical stability and for minimizing truncation errors.[4] In the pressure contribution to W [the second term in Eq. (47b)], V' is differenced to conserve the volume, thus preserving the feature that the MHD forces depend on p only through $\partial p/\partial\rho$. This is accomplished by introducing $U = R^2/2$ and writing

$$V'(k + 1/2) = \sum_i \sum_j (U_\theta Z_\rho - U_\rho Z_\theta)^{k+1/2} \Delta\theta \, \Delta\zeta,$$

$$(49)$$

where each term on the right of Eq. (49) is evaluated individually at $\rho_{k+1/2}$; for example, $U_\theta(k + 1/2) = RR_\theta(k) + RR_\theta(k + 1)$.

The quantity $\sqrt{g}|B|^2$ appearing in the magnetic field energy $W_B = W - W_p$ is evaluated at $\rho_{k+1/2}$ as follows:

$$(\sqrt{g}|B|^2)^{k+1/2} = \left(\frac{(\Phi')^2}{\mu_0 G}\right)^{k+1/2} \left(\frac{b^2(k) + b^2(k+1)}{2}\right),$$

$$(50a)$$

where

$$G(k + 1/2) = (R_\theta Z_\rho - R_\rho Z_\theta)^{k+1/2}, \quad (50b)$$

$$b^2(k) = (b_\theta^2 \hat{g}_{\theta\theta} + 2b_\theta b_\zeta \hat{g}_{\theta\zeta} + b_\zeta^2 \hat{g}_{\zeta\zeta})^k, \quad (50c)$$

$\hat{g}_{ij}(k) \equiv g_{ij}(k)/R(k)$ are the normalized metric coefficients, $b_\theta(k) = \iota(k) - \lambda_\zeta(k)$, $b_\zeta(k) = 1 + \lambda_\theta(k)$, and $\iota(k)$ is the discrete rotational transform profile. The ratio Φ'/G, which is proportional to the toroidal magnetic field, has been differenced on the half-grid to preserve the slowly varying radial behavior of this physical variable.

Using these expressions to complete the discretization of W in Eq. (47a) and taking a time derivative yields

$$\frac{dW}{dt} = -\sum_{i,j,k} [A_\alpha(k) - imB_\alpha(k) + inC_\alpha(k)]$$

$$\times \Psi_{mn} \dot{X}_\alpha^{mn}(k) \Delta\rho \, \Delta\theta \, \Delta\zeta, \quad (51)$$

where $\Psi_{mn} \equiv \exp[i(m\theta_{i-1/2} - n\zeta_{j-1/2})]$. The coefficients A, B, and C at interior radial mesh points are

$$A_R(k) = \frac{(Z_\theta P)^{k+1/2} - (Z_\theta P)^{k-1/2}}{\Delta\rho} + (RZ_\theta)^k p'(k)$$

$$+ \Phi_k^* \left(\frac{b^2(k)}{2R(k)} - b_\zeta^2(k)\right), \quad (52a)$$

$$B_R(k) = -\tfrac{1}{2}[(Z_\rho P)^{k+1/2} + (Z_\rho P)^{k-1/2}] + (b_\theta b_R)^k, \quad (52b)$$

$$C_R(k) = (b_\zeta b_R)^k, \quad (52c)$$

$$A_Z(k) = \frac{(R_\theta P)^{k-1/2} - (R_\theta P)^{k+1/2}}{\Delta\rho} - (RR_\theta)^k p'(k), \quad (52d)$$

$$B_Z(k) = \tfrac{1}{2}[(R_\rho P)^{k+1/2} + (R_\rho P)^{k-1/2}] + (b_\theta\, b_Z)^k, \tag{52e}$$

$$C_Z(k) = (b_\zeta b_Z)^k, \tag{52f}$$

$$A_\lambda(k) = 0, \tag{52g}$$

$$B_\lambda(k) = \widehat{\Phi}_k(b_\theta\, \hat{g}_{\theta\zeta} + b_\zeta\, \hat{g}_{\zeta\zeta})^k, \tag{52h}$$

$$C_\lambda(k) = -\widehat{\Phi}_k(b_\theta\, \hat{g}_{\theta\theta} + b_\zeta\, \hat{g}_{\theta\zeta})^k. \tag{52i}$$

Here,

$$\Phi_k^* = \frac{1}{2\mu_0}\left[\left(\frac{(\Phi')^2}{G}\right)^{k+1/2} + \left(\frac{(\Phi')^2}{G}\right)^{k-1/2}\right], \tag{53a}$$

$$\widehat{\Phi}_k = \frac{1}{4\mu_0}[(\Phi')^{k+1/2} + (\Phi')^{k-1/2}]$$
$$\times\left[\left(\frac{\Phi'}{G}\right)^{k+1/2} + \left(\frac{\Phi'}{G}\right)^{k-1/2}\right], \tag{53b}$$

$$b_R(k) = \frac{\Phi_k^*}{R(k)}(b_\theta\, R_\theta + b_\zeta\, R_\zeta)^k, \tag{53c}$$

$$b_Z(k) = \frac{\Phi_k^*}{R(k)}(b_\theta\, Z_\theta + b_\zeta\, Z_\zeta)^k, \tag{53d}$$

$$P^{k+1/2} = \frac{1}{4\mu_0}\left[\left(\frac{\Phi'}{G}\right)^2\right]^{k+1/2}[b^2(k) + b^2(k+1)]. \tag{53e}$$

The discrete variational procedure yields Φ_k^*, instead of $\widehat{\Phi}_k$, in Eqs. (52h) and (52i). Departure from the rigorous variational result is introduced to preserve the correct asymptotic behavior for the discretized λ as $\rho \to 0$.

At the origin, the correct discrete expressions for the forces can be obtained by integrating Eq. (18) from $\rho = 0$ to $\rho = \Delta\rho/2$. The asymptotic forms for R, Z, and λ at the magnetic axis, which were derived in Sec. V, can then be used to obtain the following expressions:

$$A_R(1) = \frac{2(Z_\theta P)^{3/2}}{\Delta\rho} + \Phi_1^*\left(\frac{\hat{g}_{\zeta\zeta}(1)}{2R(1)} - 1\right), \tag{54a}$$

$$C_R(1) = [\Phi_1^*/R(1)]R_\zeta(1), \tag{54b}$$

$$A_Z(1) = 2(R_\theta P)^{3/2}/\Delta\rho, \tag{54c}$$

$$C_Z(1) = [\Phi_1^*/R(1)]Z_\zeta(1), \tag{54d}$$

where

$$\Phi_1^* = [(\Phi')^2/2\mu_0 G]^{3/2}, \tag{54e}$$

and $P^{(3/2)}$ is given by Eq. (53e) for $k = 1$. Note that $b^2(1) = \hat{g}_{\zeta\zeta}(1)$, and $B_R(k)$ and $B_Z(k)$ do not contribute to the $m = 0$ force components [since they are multiplied by im in Eq. (51)]. The result in Eq. (54) differs from the variational discretization by the factor of 2 appearing in the radial derivative terms of A_R and A_Z. This discrepancy can be traced to the inadequacy of the differencing scheme for $|B|^2$ in Eq. (50a) as $\rho \to 0$.

At the plasma boundary $\rho_k = 1$, either R and Z are prescribed for a fixed-boundary equilibrium, or $P(b) = R(b)|\nabla\Phi|^2(b)/2\mu_0$ (where b denotes the boundary) can be used in Eq. (52) for a free-boundary equilibrium. The λ force may be obtained by using backward differences for R_ρ and Z_ρ to evaluate $G(b)$. Then B_λ and C_λ have the same forms as

those given in Eq. (52), with $\widehat{\Phi}$ replaced by

$$\widehat{\Phi}(b) = (\Phi_b')^2/\mu_0\, G(b). \tag{55}$$

Here, $G(b) = R_\theta(b)Z_\rho(b) - R_\rho(b)Z_\theta(b)$, where $Z_\rho(b)\simeq Z_\rho(N_\rho - 1/2)$ and $R_\rho(b)\simeq R_\rho(N_\rho - 1/2)$.

Comparing Eqs. (52)–(54) with Eq. (18), it is apparent that A_α arises from the ρ derivative terms in the MHD forces (together with the centrifugal force in F_R), and B_α and C_α arise from the total θ and ζ derivative terms, respectively. The coefficient of $\dot{X}_\alpha^{mn}(k)$ in Eq. (51) yields the following nodal equations for the discrete Fourier-transformed MHD forces:

$$(V_i')F_\alpha^{mn}(k) = A_\alpha^{mn}(k) + imB_\alpha^{mn}(k) - inC_\alpha^{mn}(k), \tag{56}$$

where $A_\alpha^{mn}(k) \equiv \Sigma_{i,j}\, A_\alpha(k)\Psi_{mn}^*\, \Delta\theta\, \Delta\zeta$ is the discrete Fourier transform of $A_\alpha(k)$.

VIII. GALERKIN METHOD FOR MAGNETIC AXIS

Because of the singular behavior of the force equations in the neighborhood of the magnetic axis, it was necessary in the previous section to modify the discretization process as $\rho \to 0$. As the number of Fourier mode amplitudes increases, there is a greater sensitivity to small numerical errors in the position of the axis, as well as the plasma shift, so that the convergence of the descent algorithm is adversely affected. Improved numerical stability of the descent iteration can be realized by applying the Galerkin method to the axis shift components,

$$R_0(\zeta, \rho) \equiv \frac{1}{2\pi}\int R\, d\theta = \sum_n R^{0n}(\rho)\exp(-in\zeta), \tag{57a}$$

$$Z_0(\zeta, \rho) \equiv \frac{1}{2\pi}\int Z\, d\theta = \sum_n Z^{0n}(\rho)\exp(-in\zeta), \tag{57b}$$

comprising the $m = 0$ Fourier components of R and Z. The method consists of expanding the Fourier amplitudes R^{0n} and Z^{0n} in the polynomial series in ρ, rather than discretizing them on a radial mesh. The improved numerical properties associated with this Galerkin procedure arise from two features of the method: (1) the magnetic axis $R_0(\zeta,0)$, $Z_0(\zeta,0)$ is now determined by an average force balance over ρ, rather than by the force at the singular point $\rho = 0$ alone; and (2) the radial variation of R_0, Z_0 will be smooth as a function of ρ, thus guaranteeing a well-behaved Jacobian $\sqrt{g}$ (which is strongly affected by the radial gradients of R_0, Z_0).

Let X_j^{0n} denote R^{0n} or Z^{0n} for $j = 1$ or 2, respectively. Then

$$X_j^{0n}(\rho) = \sum_{k=0} c_{nk}^j u_k(\rho), \tag{58a}$$

where $u_k(\rho) = \sqrt{4k+1}\, P_{2k}(\rho)$ and P_{2k} is the Legendre polynomial of order $2k$. This choice of basis functions was motivated by noting that $u_k'(0) = 0$ satisfies the boundary condition Eq. (27b) at the magnetic axis. The u_k are orthonormal polynomials on the interval $\rho = [0,1]$ with unit weight function. Since the boundary condition $X_j^{0n}(1) = X_{jb}^{0n}$ may be prescribed, the c_{nk}^j are not independent but satisfy $\Sigma_{k=0}\sqrt{4k+1}\, c_{nk}^j = X_j^{0n}(1)$. Using this relation to elimi-

S. P. Hirshman and J. C. Whitson   3562

nate c^j_{n0} yields an unconstrained Galerkin expansion for X^{0n}_j:

$$X^{0n}_j(\rho) = X^{0n}_j(1) + \sum_{k=1} c^j_{nk} \hat{u}_k(\rho), \qquad (58b)$$

where $\hat{u}_k(\rho) = \sqrt{4k+1} \, [P_{2k}(\rho) - 1]$. Inserting this expansion into Eq. (21a) for $\dot{W}$ yields descent equations for c^j_{nk}:

$$\dot{c}^j_{nk} = \int_0^1 \hat{u}_k \, F^{0n}_j \, dV. \qquad (59)$$

Obviously, the expansion coefficients are determined by radially weighted averages of the MHD residual forces.

For the examples discussed in the next section, the Galerkin method has been used when mode convergence studies, requiring many Fourier modes, were performed. In all instances examined so far, the Galerkin approach has been as accurate as, but more stable than, the discretization method when increasing numbers of Fourier modes are retained. Also, good radial resolution is generally achieved by retaining only two or three expansion coefficients in the series, Eq. (58b).

IX. NUMERICAL EXAMPLES

Some numerical results obtained using the method described in the previous sections are now presented. In all the examples, the effect of the angle renormalization parameter λ is substantial. A symmetry property of particular prevalence in stellarator designs, which permits a reduction in the number of equilibrium equations, has been used to obtain these numerical results. Many systems of practical interest possess at least one toroidal plane ($\phi = 0$, specifically) where the coil symmetry imposes a flux surface shape with vertical symmetry. In this plane, $R(\rho, \theta, 0) = R(\rho, -\theta, 0)$ and $Z(\rho, \theta, 0) = -Z(\rho, -\theta, 0)$. By analytic continuation, this symmetry property implies the following Fourier series for
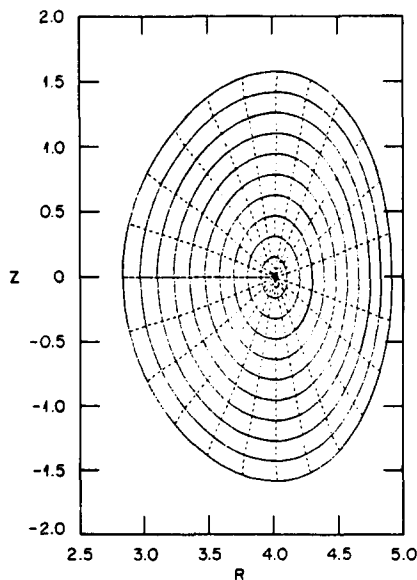

FIG. 3. Normalized profiles $\bar{R}_m = R_{m0}/R^*_m$ and $\bar{Z}_m = Z_{m0}/Z^*_m$ for Solov'ev equilibrium, where $R^*_0 = 3.999$, $R^*_1 = 1.026$, $R^*_2 = 0.068$, $Z^*_1 = 1.58$, and $Z^*_2 = 0.01$.

R, Z for *all* values of ϕ:

$$R(\rho, \theta, \phi) = \sum_{m,n} R^{mn}(\rho)\cos(m\theta - n\phi), \qquad (60a)$$

$$Z(\rho, \theta, \phi) = \sum_{m,n} Z^{mn}(\rho)\sin(m\theta - n\phi). \qquad (60b)$$

Thus, half the possible terms in the general Fourier expansion of R, Z have been eliminated by symmetry. Furthermore, by examining the structure of the F_λ operator defined in Eq. (14b), it is possible to infer that

$$\lambda(\rho, \theta, \phi) = \sum_{m,m} \lambda^{mn}(\rho)\sin(m\theta - n\phi). \qquad (60c)$$

Figures 2–4 show the flux surfaces, normalized Fourier amplitudes, and residual decay, respectively, for the particular 2-D Solov'ev equilibrium discussed in Ref. 4. With a radial mesh of 10–20 points, a discretization error of less than 0.1% in the value of $R_0(0)$ (which should be 4) was obtained using more than two harmonics for R, Z, and λ. For the

FIG. 2. Flux surfaces for Solov'ev equilibrium $(R/4)^2 = 1 - (\rho/2)\cos\theta$, $Z = (\sqrt{10}/2)\sin\theta, p = (1 - \rho^2)/8$, and $\chi = \rho^2$.
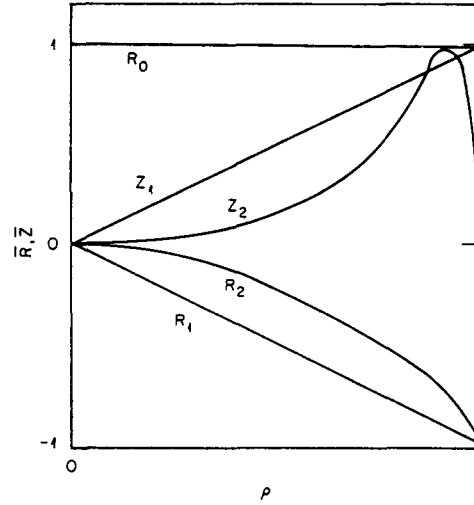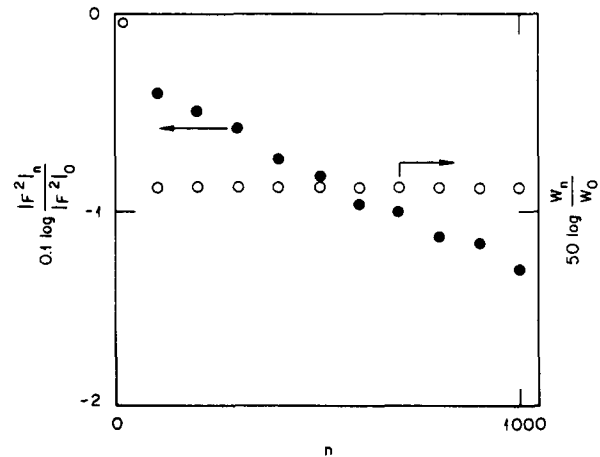

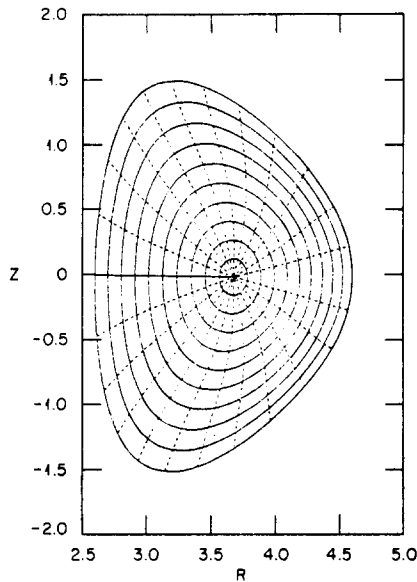FIG. 4. Residual decay and change in energy as a function of iteration number for Solov'ev equilibrium.

FIG. 5. Flux surfaces for high-beta, D-shaped plasma, $\langle \beta \rangle \simeq 0.03$, with $R_b = 3.51 - \cos \theta + 0.106 \cos 2\theta$, $Z_b = 1.47 \sin \theta + 0.16 \sin 2\theta$.

example shown, a total of 12 harmonic amplitudes was re-tained (although a minimum of six harmonics produces es-sentially the same flux surface configurations). In Fig. 2, the solid lines represent the magnetic surfaces and the dashed lines correspond to constant θ contours. Note that after the first 100 iterations the energy has already converged to with-in three significant figures, whereas the residuals $|F^2| \equiv \int F^2 \, dV$ (which are normalized to W) continue to de-cay at a more or less uniform rate.

Figures 5–7 illustrate the same features for a high-beta ($\langle \beta \rangle = 3\%$), axisymmetric, D-shaped plasma. The pressure profile was taken to be $p = p_0(1 - \rho^2)^2$ and the rotational transform was given by $\iota = 1 - 0.67\rho^2$. Because the Jacobi-an for the D-shaped configuration is not uniform with re-spect to the poloidal angle θ, there is a substantial decrease in
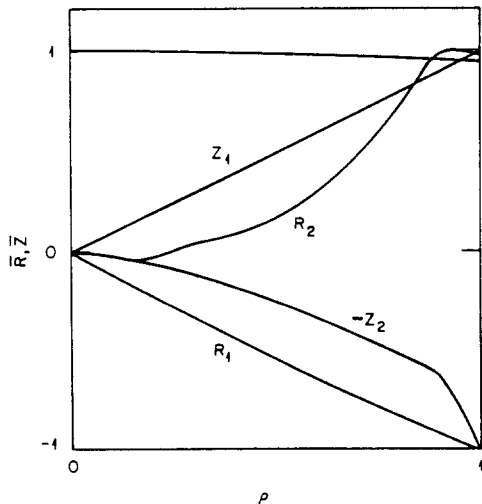

FIG. 6. Normalized profiles $\bar{R}_m = R_{m0}/R_m^*$ and $\bar{Z}_m = Z_{m0}/Z_m^*$ for high-beta, D-shaped plasma, with $R_0^* = 3.97$, $R_1^* = 1.00$, $R_2^* = 0.107$, $Z_1^* = 1.47$, and $Z_2^* = 0.16$.
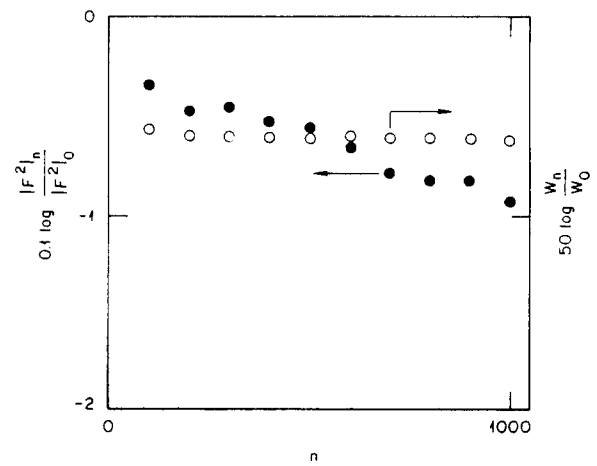

FIG. 7. Residual decay and change in energy as a function of iteration num-ber for the high-beta, D-shaped plasma.

the *rate* of residual decay in this case compared with the Solov'ev equilibrium for which $\partial \sqrt{g}/\partial \theta = 0$ [see Eq. (38)]. The figures correspond to a total of 12 poloidal harmonics, although convergence has been achieved with up to 30 har-monics. This limited convergence study indicates that after a certain minimum number of harmonics is present, the values of the lowest-order harmonics seem to remain invariant to the addition of further harmonics.

Figures 8–10 present the flux surface and residual decay for the heliotron model configuration,[16] which has an outer boundary ($\rho = 1$)

$$R = 10 - \cos \theta - 0.3 \cos(\theta - N\zeta), \tag{61a}$$

$$Z = \sin \theta - 0.3 \sin(\theta - N\zeta), \tag{61b}$$

where $N = 19$ is the number of field periods. A total of 18 mode amplitudes (six modes each for R, Z, and λ, corre-sponding to all combinations of $m = 0, 1, 2$ and $n = 0, N$) was used to obtain the equilibrium configurations shown. Here, the pressure is $p = p_0(1 - \rho^2)^2$, and $\iota = 0.5 + 1.5\rho^2$. The low-beta result shows the approximate vacuum topol-ogy, whereas at high beta ($\langle \beta \rangle = 2\%$), a substantial Sha-franov shift $\Delta \sim 0.2$ is apparent. To obtain the residual decay shown in Fig. 10 for $\langle \beta \rangle = 2\%$ took about 32 sec of CPU time on the CRAY computer. The results of a beta scan are summarized in Fig. 11, where the average toroidal shift $\Delta R = (R_{00} - 10)$ is displayed versus $\langle \beta \rangle$. This is in approxi-mate agreement with the free boundary calculations report-ed in Ref. 16.

Finally, Figs. 12 and 13 represent the flux surfaces for the Advanced Toroidal Facility (ATF)[17] model configura-tion, with an outer boundary (in meters):

$$R = 2.05 - 0.29 \cos \theta + 0.09 \cos(\theta - N\zeta)$$
$$+ 0.125[\cos 2\theta - \cos(2\theta - N\zeta)], \tag{62a}$$

$$Z = 0.29 \sin \theta + 0.09 \sin(\theta - N\zeta)$$
$$+ 0.00675[\sin 2\theta - \sin(2\theta - N\zeta)], \tag{62b}$$

where $N = 12$. The pressure was chosen to be $p = p_0(1 - \rho^2)^2$, and $\iota = 0.35 + 0.65\rho^2$. In Eq. (62), the ($\cos \theta$, $\sin \theta$) terms produce an axisymmetric circular plas-ma and the [$\cos(\theta - N\zeta)$, $\sin(\theta - N\zeta)$] terms represent a he-

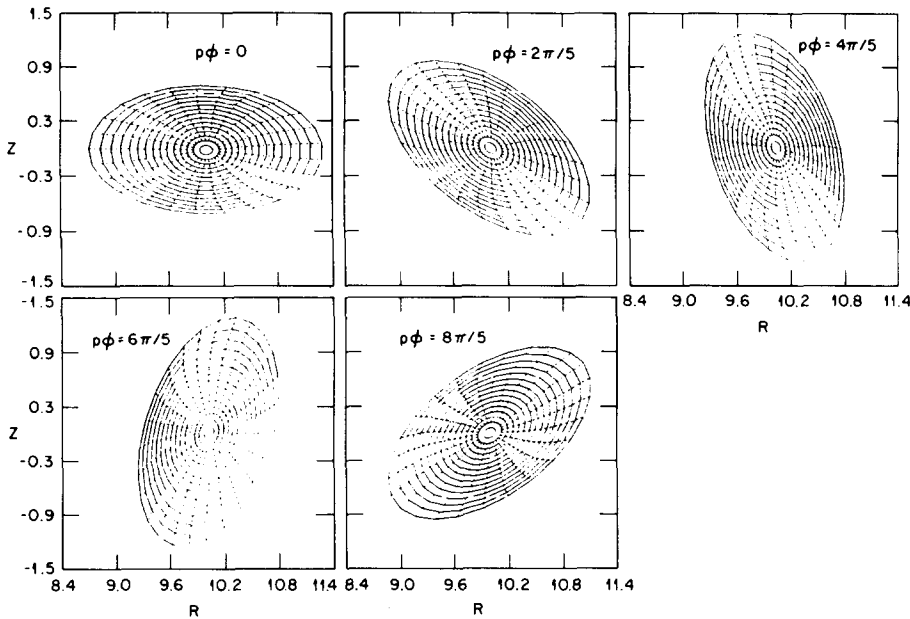S. P. Hirshman and J. C. Whitson   3564

FIG. 8. Low-beta ($\langle \beta \rangle = 0.1\%$) flux surfaces for heliotron model configuration.

lically varying elliptical distortion. The last terms in Eq. (62) describe the D-shaped distortion of the plasma most notable in Figs. 12 and 13 at $N\zeta = \pi$. At the higher $\langle \beta \rangle$ value, a marked helical distortion ($\cos N\zeta$, $\sin N\zeta$ terms) of the magnetic axis develops, even though there is no pure helical modulation of the boundary surface. Figure 14 shows the mean toroidal axis shift $\Delta R = (R_{00} - 2.05)$ vs $\langle \beta \rangle$ for this ATF model, which is in good agreement with the results obtained in Ref. 17.

ACKNOWLEDGMENTS

APPENDIX: OPTIMAL CHOICE FOR THE POLOIDAL ANGLE

The rate at which a magnetic flux surface is traversed in the poloidal direction can be chosen independent of its shape. This leads to the interdependence of the MHD forces F_R, F_Z, and F_λ when the renormalization parameter λ is introduced. This degeneracy may be resolved by specifying the poloidal angle θ. Several choices for θ have been discussed in the literature.[4,5,7,18] In this Appendix, it is argued that the requirement of rapid convergence for the Fourier moment expansions of R and Z selects a particular angle θ that has not been previously considered.

One choice[4] for θ is a polar representation for which $\theta = \tan^{-1}(\bar{Z}/\bar{R})$, where $(\bar{R}, \bar{Z})$ are local Cartesian coordinates (in the plane $\phi = \text{const}$) measured from the magnetic axis. In this system, Eq. (16) is replaced by a single equation
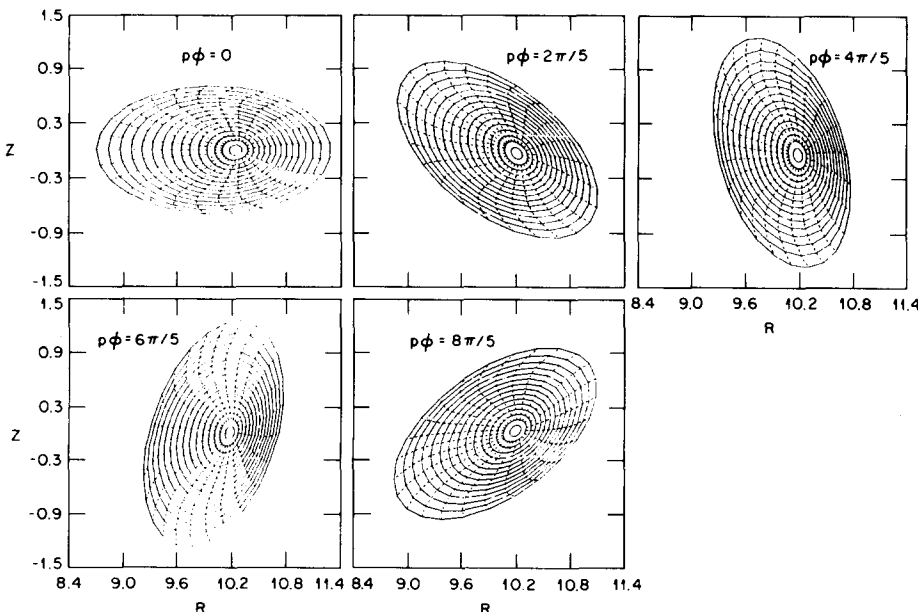

FIG. 9. High-beta ($\langle \beta \rangle = 2\%$) flux surfaces for heliotron model configuration.
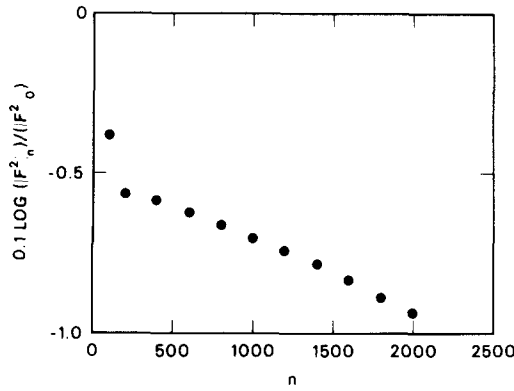
FIG. 10. Residual decay for the high-beta heliotron configuration.

FIG. 11. Toroidal shift ΔR vs $\langle \beta \rangle$ for heliotron configuration.

$\dot{r} \sim F_\rho$, where $r = (\overline{R}^2 + \overline{Z}^2)^{1/2}$ is the polar radius. Because $r(\rho, \theta, \zeta)$ must be a single-valued function of the flux coordinates, this representation is limited to star-like domains (or boundary shapes that can be mapped into star-like domains) and cannot describe, for example, strongly pinched surfaces that might appear in a plasma preceding the development of magnetic islands. In addition, the polar angle θ may not lead to a rapidly convergent Fourier expansion of r. (This difficulty poses no problem in Ref. 4, where Fourier analysis is not used.) For example, an elliptical flux surface $\overline{R}^2 + \overline{Z}^2/\kappa^2 = 1$ becomes (for $\kappa \geqslant 1$) $r = [1 - (1 - \kappa^{-2}) \times \sin^2 \theta]^{-1/2}$, which develops a significant Fourier spectrum as κ departs from unity. The same problem exists for certain other angle choices. For example, the angle producing equal arc lengths around a flux surface requires $\partial g_{\theta\theta}/\partial\theta = 0$ and has a substantial Fourier spectrum even for the simplest noncircular geometric shapes.

To avoid the restriction to star-like domains imposed on the polar system, the cylindrical system (R, ϕ, Z) was introduced in Sec. III. In this system, a natural unique choice[7,18] for the poloidal angle is $\theta = \theta^*$, where θ^* is the angle that, together with $\zeta = \phi$, defines a straight magnetic
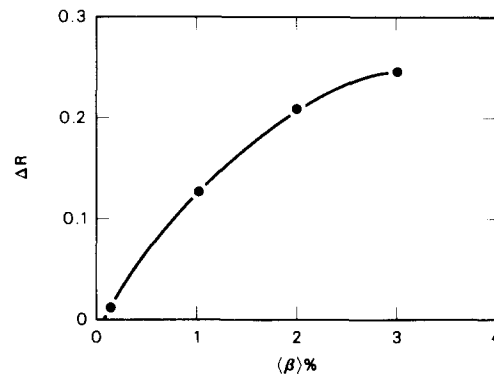
field line coordinate system. Although this choice for θ is adequate in the context of Ref. 18, where the MHD equilibrium equations are solved on a Lagrangian grid, it is generally inappropriate for use in conjunction with Fourier analysis. (An explicit analytic example of this is given in Sec. VI.) The poor convergence properties associated with θ^* may be understood by considering a fixed plasma boundary with the following finite parametric representation:

$$R_b(\theta, \zeta) = \sum_{m=0}^{M_R} \sum_{n=-N_R}^{N_R} R^{mn} \cos(m\theta - n\zeta), \qquad \text{(A1a)}$$

$$Z_b(\theta, \zeta) = \sum_{m=0}^{M_Z} \sum_{n=-N_Z}^{N_Z} Z^{mn} \sin(m\theta - n\zeta). \qquad \text{(A1b)}$$

It is assumed that Eqs. (A1) are the most economical series representations of the boundary, in the sense that any periodic displacement of θ increases the total number of harmonics, $M_R N_R + M_Z N_Z$. Note that the shape of the boundary, at a fixed toroidal angle ζ, is invariant to such displacements, which merely change the rate at which the boundary is traversed as θ increases. In general, the parametric (geometric) angle θ in Eqs. (A1) does not coincide with θ^*. (Even if θ and θ^* agreed initially, it would be impossible
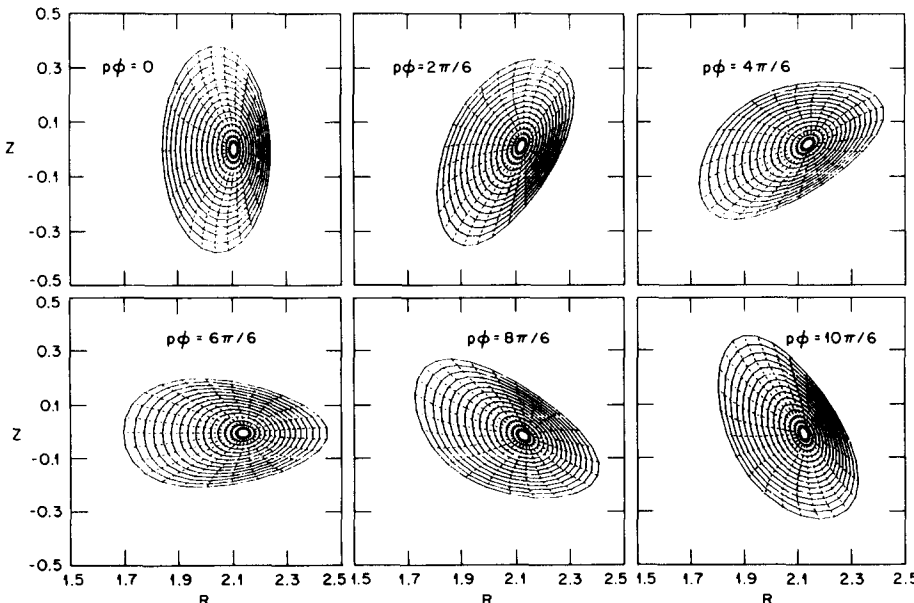

FIG. 12. Moderate-beta ($\langle \beta \rangle = 2\%$) flux surfaces for ATF model configuration.
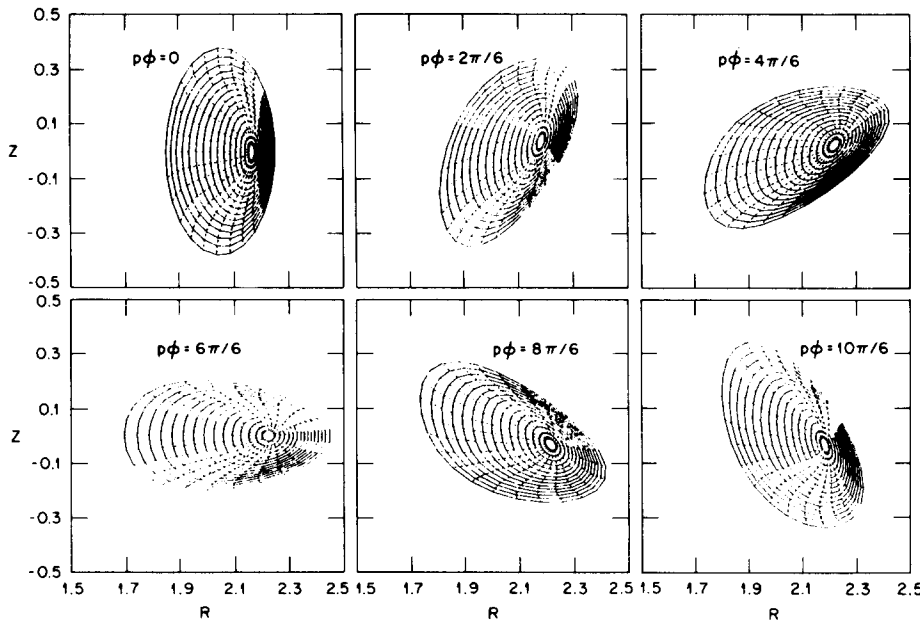
FIG. 13. High-beta ($\langle \beta \rangle = 8\%$) flux surfaces for ATF model configuration.

to guarantee their equality as the plasma evolved toward equilibrium. This is because the operator F_λ, which determines the evolution of θ^*, depends on $\sqrt{g}$, which is not a function of the boundary coordinates alone.) Thus, in terms of $\theta^* = \theta + \lambda_b^*(\theta^*, \zeta)$, where λ_b^* is a periodic function, Eq. (A1a) becomes (with a similar result for Z_b)

$$R_b(\theta^*, \zeta) = \sum_{m=0}^{M_R} \sum_{n=-N_R}^{N_R} R^{mn} \cos[m(\theta^* - \lambda_b^*) - n\zeta]$$

$$= \sum_{m=0}^{M_*^*} \sum_{n=-N_*^*}^{N_*^*} R_*^{mn} \cos(m\theta^* - n\zeta), \qquad (A2)$$

where $M_R^* N_R^* + M_Z^* N_Z^* > M_R N_R + M_Z N_Z$. Not only is the number of Fourier harmonics in general (substantially) increased in the θ^* system, but also the boundary coefficients R_*^{mn} are no longer constant during the energy minimization even for a fixed boundary equilibrium. Rather, they undergo[18] periodic Lagrangian displacements along the boundary curve that are of the form $\delta R_b = R_\theta \lambda$ and $\delta Z_b = Z_\theta \lambda$, with $\lambda = -F_\beta$. Thus, simply to conserve the outer boundary shape requires a large number of harmonics in the θ^* system. For these reasons, it is preferable to transform to the geometric coordinate system $\theta = \theta^* - \lambda_b^*$, where the boundary Fourier coefficients *can* be fixed and

FIG. 14. Toroidal shift ΔR vs $\langle \beta \rangle$ for ATF configuration.

where the number of harmonics is minimized. Because of the large number of harmonics generated by the transformation to θ^* in Eq. (A2), it may be concluded that the development in Ref. 7, though technically correct, is of little practical importance.

Having transformed to θ at the boundary, it becomes necessary to extend this coordinate system into the plasma. This is exactly what Eq. (3a) accomplishes. The coefficients (R^{mn}, Z^{mn}) in Eqs. (A1) are specified boundary values. This yields a unique transformation from θ^* to θ at the boundary. However, the transformation equation (3a) is not unique in the plasma interior, where the same flux surface can have an infinite number of parametric representations under the family of transformations given by Eq. (3a). This underdetermination of θ is irrelevant in practice where only *finite* Fourier expansions are used to represent the equilibrium solutions. For finite-term series expansions of R and Z, there exists a unique poloidal angle θ (the geometric angle) that leads to the most accurate solution of the inverse equilibrium problem in the sense of convergence in the mean. (This conclusion concerning series economization follows from the Fourier–Bessel theory of finite-series approximation.) We now demonstrate that the variational principle given in Sec. III is capable of determining the geometric poloidal angle as a result of the minimization process (with fixed boundary conditions). That is, the variational principle automatically performs the series economization when the angle renormalization parameter λ is retained. As a consequence, no constraint between the Fourier harmonics need be imposed *ab initio* whenever a finite-series approximation to R and Z is sought.

To prove this remarkable property of the variational equations it suffices to show that when $\lambda \neq 0$, the equations for $\dot{R}$ and $\dot{Z}$ are independent whenever finite Fourier series approximations for R and Z are used. Without loss of generality it may be assumed that $F_\lambda = 0$ can be satisfied by an appropriate choice of λ. Then Eq. (16) yields
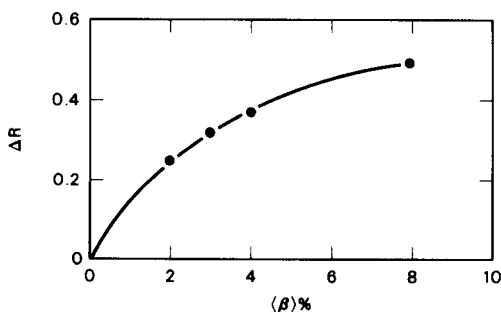
S. P. Hirshman and J. C. Whitson

$$\dot{R} = Z_\theta \, \overline{F}_\rho, \tag{A3a}$$

$$\dot{Z} = -R_\theta \, \overline{F}_\rho, \tag{A3b}$$

where $\overline{F}_\rho = RF_\rho$ is the 3-D inverse Grad–Shafranov operator. In the infinite mode number (continuous) limit, the underdetermination of θ is manifested in Eqs. (A3) by the fact that $\dot{R}$ and $\dot{Z}$ are not independent equations. However, for a finite-series expansion of R and Z, and hence of R_θ and Z_θ, the Fourier moments of the variational equations (A3) needed to extract the appropriate harmonics of $\dot{R}$ and $\dot{Z}$ yield exactly the correct number of independent equations for determining each of the harmonics of R and Z. This is due to the mode coupling produced by Z_θ and R_θ in Eqs. (A3). (It is assumed that because of the strong nonlinearity of F_ρ, the harmonics of F_ρ are independent at least up to a mode number equal to the sum of the R and Z mode numbers. Also, since $\sqrt{g} \neq 0$, R_θ and Z_θ do not both vanish.)

Because Eqs. (A3) are indeterminate in the continuous limit, they are probably ill-conditioned for finite but large mode numbers. Limited-mode convergence studies (see Sec. IX) suggest that lack of uniqueness does not seem to produce any deleterious numerical effects when used in conjunction with the steepest-descent method. This is probably due to the fact that the initial guess for (R^{mn}, Z^{mn}) is sufficient to yield a unique descent path and thus determines a unique poloidal angle even when many modes are present (up to 30 mode amplitudes have been successfully converged).

When a unique poloidal angle choice is desired, it is possible to scale λ from its value at the plasma boundary (which *is* unique) into the plasma, e.g., $\lambda = \rho\lambda_b$. In this way, the renormalization features of λ are retained, while Eqs. (A3) are no longer ill-conditioned.

[1]M. D. Kruskal and R. M. Kulsrud, Phys. Fluids **1**, 265 (1958).

[2]H. Grad, Phys. Fluids **7**, 1283 (1964).

[3]R. Chodura and A. Schlüter, J. Comput. Phys. **41**, 68 (1981).

[4]F. Bauer, O. Betancourt, and P. Garabedian, *A Computational Method in Plasma Physics* (Springer–Verlag, New York, 1978); Phys. Fluids **24**, 48 (1981).

[5]L. L. Lao, S. P. Hirshman, and R. M. Wieland, Phys. Fluids **24**, 1431 (1981).

[6]V. D. Pustovitov, V. D. Shafranov, L. E. Zakharov, L. M. Degtyarev, V. V. Drozdov, S. Y. Medvedev, and M. I. Mikhajlov, in *Plasma Physics and Controlled Nuclear Fusion Research* (IAEA, Vienna, 1982), Paper IAEA-CN-41/V-5.

[7]A. Bhattacharjee, J. C. Wiley, and R. L. Dewar (submitted to Phys. Fluids).

[8]J. M. Greene, J. L. Johnson, and K. E. Weimer, Phys. Fluids **14**, 671 (1971).

[9]S. Hamada, Nucl. Fusion **1**, 23 (1962).

[10]P. Garabedian, Math. Tables Aids Comput. **10**, 183 (1956).

[11]G. D. Smith, *Numerical Solution of Partial Differential Equations* (Oxford U. P., London, 1965).

[12]L. S. Solov'ev, Sov. Phys.-JETP **26**, 400 (1968).

[13]J. M. Ortega and W. C. Rheinboldt, *Iterative Solution of Nonlinear Equations in Several Variables* (Academic, New York, 1970), p. 21.

[14]P. J. Davis and P. Rabinowitz, *Methods of Numerical Integration* (Academic, New York, 1975), p. 106ff.

[15]S. A. Orszag, J. Comput. Phys. **37**, 70 (1980).

[16]F. Bauer, O. L. Betancourt, P. R. Garabedian, and J. L. Shohet, IEEE Trans. Plasma Sci. **PS-9**, 239 (1981).

[17]J. F. Lyon, B. A. Carreras, J. H. Harris, J. A. Rome, R. A. Dory, L. Garcia, T. C. Hender, S. P. Hirshman, T. C. Jernigan, J. Sheffield, L. A. Charlton, R. H. Fowler, H. R. Hicks, J. A. Holmes, V. E. Lynch, B. F. Masden, D. L. Goodman, and S. A. Hokin, in *Plasma Physics and Controlled Nuclear Fusion Research* (IAEA, Vienna, 1982), Paper IAEA-CN-41/Q3.

[18]A. Schlüter and U. Schwenn, Comput. Phys. Comm. **24**, 263 (1981).

3568   Phys. Fluids, Vol. 26, No. 12, December 1983

S. P. Hirshman and J. C. Whitson   3568